Russian Chemical Reviews **73** (9) 881 – 898 (2004) © 2004 Russian Academy of Sciences and Turpion Ltd

DOI 10.1070/RC2004v073n09ABEH000920

Structural and microstructural features of functional materials based on cuprates and manganites

Yu D Tretyakov, E A Goodilin, D V Peryshkov, D M Itkis

Contents

I.	Role of the d-elements in design of new materials	881
II.	Crystal structures of cuprates and manganites	882
III.	Local structure and defects	885
IV.	Chemical properties and phase diagrams	887
V.	Single crystals	889
VI.	Microstructure and new methods of preparation of ceramic composites	890
VII.	Geometrical control of mutual orientation of crystallites (graphotexturing)	892
VIII.	Fields of practical applications of cuprates and manganites	895

Abstract. The review considers characteristic features of the crystal structure, phase relations, microstructure and physical properties of the most important classes of modern cuprate and manganite materials including high-temperature superconductors, CMR magnetic semiconductors and superionic conductors. The bibliography includes 189 references.

I. Role of the d-elements in design of new materials

In design of modern functional materials possessing nonlinear magnetic and electric properties an important role is played by the transition elements capable of being in different oxidation states and spin states.[1,2] Among oxide materials, there are two most promising classes which have become the subjects of intensive research recently. These are high-temperature superconductors (HTSC)[3–8] and 'colossal magnetoresistive' (CMR) materials.[9–11] Open framework structures have also attracted close attention of researchers.[12,13] Often, these classes of compounds comprise complex oxides of copper and/or manganese. Peculiarities of the properties of these elements and their oxides are of crucial importance for practical applications because they allow one to trace how the chemical properties of the d-elements influence the functional properties of materials.

In a rather short time, large-scale research on high-temperature superconductivity has contributed largely to modern inorganic chemistry, physical chemistry, solid state chemistry and materials science.[3] High-temperature superconducting cuprates represent one of the most promising classes of ceramic materials possessing structure-sensitive properties. They are still complex and very interesting objects that are far from being studied comprehensively. Methodological approaches and experimental basis of inorganic chemistry and solid state chemistry are of particular importance for carrying out basic research on these compounds.

The ability of manganese to form complex framework structures built of joined MnO_6 octahedra and filled with different types of cations located in the framework cavities predetermines the variety of manganese-containing oxide materials.[14] For instance, hollandite, $BaMn_8O_{16}$, is one of the most prominent and well-known examples of compounds with a specific tunnel structure, which provides the possibility of using this phase as a catalyst, solid electrolyte, matrix for nuclear waste disposal and an electrode material.[13,15]

The magnetic, magnetotransport and other practically important physical properties of manganites are to a great extent governed by the ability of manganese to be present in the structure simultaneously in different oxidation states, by electron exchange between Mn^{3+} and Mn^{4+} and, sometimes, by the spin and charge ordering.[9–11] The discovery of the CMR effect in the manganites with perovskite structure, $R_{1-x}A_xMnO_{3-\delta}$ [R is a rare-earth element (REE) and A is an alkali or alkaline-earth metal[9–11]] was followed by a new flare of interest in studies of manganite systems in connection with the possibility of using them in magnetometers, reading heads for high-density magnetic recording, data storage devices, metal detectors, sensors, *etc.*[11] Perovskite-type manganites of compositions $CaCu_xMn_{7-x}O_{12}$ exhibit some features such as specific magnetoresistance mechanism different from that observed in conventional perovskites, the possibility for a rather high magnetoresistance to be achieved at relatively low magnetic fields and smooth temperature dependences of these parameters (in contrast to manganites $AMnO_3$). This offers great prospects for practical applications of these phases.[16–19] The temperature and the magnetic field dependences of the magnetoresistance indicate a large contribution of intergrain tunnelling to the total magnetoresistance of $CaCu_xMn_{7-x}O_{12}$ compounds. Generally, the tunnelling magnetoresistance depends on the microstructure, in particular, on the grain size, mutual orientation of grains and on the surface area of grain boundaries. Optimisation of these characteristics requires elaboration of novel methods of synthesis of these materials.[20] Thus, similarly to superconducting cuprates, complex oxides of alkaline-earth metals and manganese are of particular interest for inorganic chemistry and materials science.

This review concerns the main methods of preparation of modern functional materials and the 'composition – treatment –

Yu D Tretyakov, E A Goodilin, D V Peryshkov, D M Itkis Department of Chemistry and Department of Materials Science, M V Lomonosov Moscow State University, Leninskie Gory, 119992 Moscow, Russian Federation. Fax (7-095) 939 09 98. Tel. (7-095) 939 20 74.
E-mail: yudt@inorg.chem.msu.ru (Yu D Tretyakov).
Tel. (7-095) 939 47 29. E-mail: goodilin@inorg.chem.msu.ru (E A Goodilin), pyoryshkov@inorg.chem.msu.ru (D V Peryshkov), itkis@inorg.chem.msu.ru (D M Itkis)

Received 9 March 2004
Uspekhi Khimii **73** (9) 954 – 973 (2004); translated by A M Raevskiy

structure – property' correlations. We also summarise here the results of theoretical and experimental studies on fabrication of ceramic materials and coatings based on superconducting cuprates, cupromanganite-based CMR magnetic semiconductors and superionic conductors based on the manganites with framework structures.†

II. Crystal structures of cuprates and manganites

The main structureal types of superconducting cuprates are as follows:

oxygen-deficient perovskites characterised by the presence of 'infinite CuO_2 layers' separated by (La,Ca) – vacancy layers [*e.g.*, (Sr,Ca)CuO_2, see Fig. 1 *a*], substitution solid solutions $Nd_{1+x}Ba_{2-x}Cu_3O_z$ based on the triple perovskite-type unit cell CuO_{1-z} – BaO – CuO_2 – Nd – CuO_2 – BaO – CuO_{1-z} with different types of ordering of the heavy cations and the oxygen sublattice (Fig. 1 *b*,*c*);

intergrowth structures characterised by intergrowth of the perovskite units containing superconducting CuO_2 planes, NaCl [*e.g.*, La_2CuO_4 (Fig.1 *d*), $Bi_2Sr_2CaCu_2O_8$ (Fig. 1 *e*), $Pb_2SrYCu_3O_8$], fluorite bloks, *etc.*;

homologues, *i.e.*, phases with different numbers of CuO_2 layers [*e.g.*, $HgBa_2CaCu_2O_{6+z}$ and $HgBa_2Ca_2Cu_3O_{8+z}$ phases (Fig. 1 *f*)] or CuO layers (*e.g.*, $RBa_2Cu_3O_7$, $R_2Ba_4Cu_7O_{14}$, $RBa_2Cu_4O_8$);

low-dimensional structures formed by differently joined planar CuO_2 units [*e.g.*, $Sr_{14}Cu_{24}O_{48}$ (Fig. 1 *g*), $Sr_2Cu_3O_5$ (Fig. 1 *h*), $LaCuO_{2.5}$ (Fig. 1 *i*)].

Almost all HTSC are complex layered copper-containing oxides containing oxygen-deficient perovskite-type structural fragments.[5,7,8,106–108] The structure and properties of the HTSC are strongly influenced by the Jahn – Teller effect and ordering of ions.[3,7,8] The former effect is responsible for the formation of low-coordinated copper polyhedra in the structure while the latter causes local distortions and charge transfer between structural blocks.

In a planar CuO_2 layer the copper atoms form a square network while the oxygen atoms are located on the lines connecting the sites of the copper atoms. The $3d_{x^2-y^2}$ electrons of the copper atoms and the $2p_{x,y}$ electrons of the oxygen atoms form the in-plane bonds in the layer. These electrons are delocalised and do not belong to a particular atom. Below the critical temperature, superconductivity arises on 'doping' the CuO_2 layers with an optimum amount of charge carriers[6] in the absence of strong structural distortions. The phases with nearly ideal planar CuO_2 layers are, *e.g.*, mercury-containing[106] HTSC and 'infinite-layer' structures.[8] The onset of superconductivity requires that the formal oxidation state of copper in the layers containing shared electrons be in the ranges from +2.05 to +2.25 (hole-doped superconductors) or from +1.8 to +1.9 (electronic superconductors). The length of the in-plane Cu – O bond must be 0.19 to 0.197 nm provided that the distance between adjacent copper atoms is 0.380 to 0.394 nm. For any member of a homologous series the dependence of T_c on the charge carrier concentration passes through an extremum, while the highest transition temperature is usually observed for the homologue with an optimum number of the superconducting planes.[21,107]

It is believed that transition to the superconducting state occurs as a result of formation of a Cooper pair (a boson) provided that the motion of two charge carriers is correlated.[108] In the early stage of research into the HTSC mechanism it was assumed that the Cooper pair is a pair of holes that polarise the lattice. The electron – phonon interaction and symmetry of the ordering parameters in terms of the Ginzburg – Landau superconductivity theory (d-, s- or mixed type) are still the subject of wide speculation.[109] At present, the most probable mechanism of superconductivity considers a two-hole charge carrier and magnetically ordered spin moments of the copper atoms in the localisation region of the Cooper pair (sometimes, this is called a magnetic polaron or a 'spin bag'). In this case the coherence length of the charge-carrier wave function is rather small and different along the main crystallographic directions.[108] The Bose 'liquid' flows through a HTSC crystallite without dissipation provided that the critical current density (the critical magnetic field) is not exceeded; otherwise, the Cooper pairs are destroyed and the HTSC passes to the normal (resistive) state.

The structures of famous superconductors are built of alternating CuO_2 planes and 'dielectric' BaO, SrO, TlO, BiO, PbO, HgO, $Ca^{\square}$, *etc.*, layers.[5,7,8,107] In the intergrowth structures the non-superconducting units often act as specific charge reservoirs that ensure the formation and transfer of charge to the superconducting planes by insertion (or removal) of extra oxygen and by heterovalent doping. This is responsible for crucial importance of another structural parameter, *viz.*, the length of the bond between the copper atoms and oxygen atoms in the neighbouring layers. These bonds are usually much longer (more than 0.22 nm) than the in-plane bonds. In other words, the structures of superconducting cuprates contain unequal chemical bonds Cu – O, namely, strong bonds in the plane of the CuO_2 layer and much weaker bonds perpendicular to these layers.

The 'infinite-layer' superconducting structures obtained under high pressure[8] (see Fig. 1 *a*) and 'ladder'-type cuprates (see Fig. 1 *g* – *i*)[110,111] are of interest from the standpoint of both fundamental superconductivity theory and crystal chemistry. Both families of cuprates are low-dimensional, strongly correlated systems built of differently connected planar $(CuO_2)_n$ units with variable dimension (1D – 2D) and width (in the case of ribbon-like structures). As a consequence. they exhibit unique features of the spin and magnetic interactions.

The structure types characteristic of manganites are as follows: perovskite [$CaMnO_3$ (Fig. 2 *a*)], spinel [Li_2MnO_4 (Fig. 2 *b*)]; homologues, Ruddlesden – Popper phases $(R_{1-x}A_x)_{n+1}Mn_nO_{3n+1}$ [R is a rare-earth element and A is an alkali-earth element; $n = 1$ (Fig. 2 *c*) and 2 (Fig. 2 *d*)] characterised by intergrowth of different numbers of perovskite-type blocks $(R_{1-x}A_x)MnO_3$ and $NaCl(R_{1-x}A_x)O$ units; layered and chain manganites [birnessite $K_{0.5}Mn_2O_{4.3}(H_2O)_{0.5}$ (Fig. 2 *e*) and $Ba_6Mn_5O_{16}$ (Fig. 2 *f*)]; and tunnel structures related to pyrochlore [$Tl_2Mn_2O_7$ (Fig. 2 *g*)], pyrolusite [β-MnO_2 (Fig. 2 *h*)], hollandite [$A_{2-x}Mn_8O_{16}$, where A = Ba, Sr, Ca, *etc.* (Fig. 2 *i*)], todorokite [$MMn_6O_{12}\cdot 3H_2O$, where M = K, Ca, Mn, *etc.* (Fig. 2 *j*)], ramsdelite R-MnO_2 (Fig. 2 *k*) and psylomelane [$Ba_{0.66}Mn_5O_{10}(H_2O)_{1.35}$ (Fig. 2 *l*)].

Most simple manganese oxides have framework or layered structures (see Fig. 2).[2,12] The oxide Mn_3O_4 has a distorted spinel structure at room temperature which undergoes a transition in the cubic polymorph (γ-Mn_3O_4) at temperatures above 1170 °C. In the structure of hausmannite (β-Mn_3O_4) the distance from the cation to each of the two anions along the [001] direction is 16% longer than the distance from the cation to any anion in the (001) plane (at room temperature). Compounds γ-Mn_2O_3 and Mn_3O_4

† These investigations are carried out by the research staff of the Department of Chemistry, M V Lomonosov Moscow State University, in collaboration with domestic and foreign research centres. The research avenues are as follows: crystal chemistry of HTSC[21–23] and modification (fluorination)[24–30] of the superconducting phases and CMR manganites; synthesis of homologues of mercury-containing HTSC[31–38] and determination of their crystal chemical features[39–42] and physical properties;[43–45] single-crystal structure refinements;[46–48] studies on thermodynamics of HTSC systems[49,50] including mercury-containing HTSC;[51,52] studies on non-stoichiometry (with respect to oxygen) in and phase stability of manganites;[53] preparation of microcomposites based on bismuth-containing HTSC phases,[54–57] CMR manganite ceramics;[58–61] fabrication of thin films and heterostructures[62–71] based on HTSC or CMR manganites with preset microstructure and defect content;[72–82] studies on giant isotope effect[83–86] and magnetooptical properties of manganites;[87–90] stabilisation effect in film structures;[91] and determination of the local structure of complex oxide phases.[92–95] Detailed reports on the research avenues mentioned above can be found in Refs 5, 11, 96 – 107.

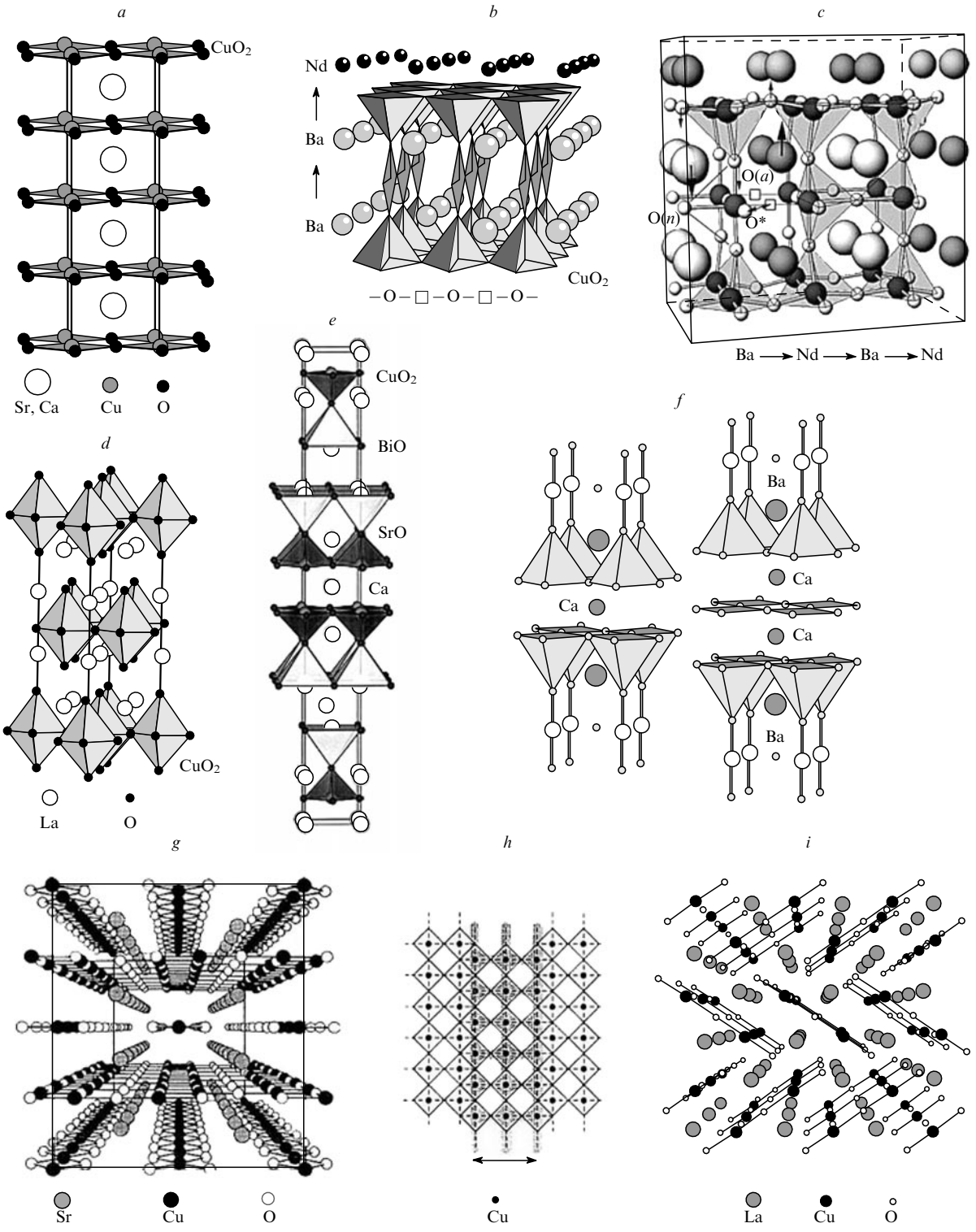


Figure 1. Main structures of superconducting cuprates.[7,8] (Sr, Ca)CuO_2 (*a*), $NdBa_2Cu_3O_z$ (*b*), $Nd_2BaCu_3O_z$ (*c*), La_2CuO_4 (*d*), $Bi_2Sr_2CaCu_2O_8$ (*e*), $HgBa_2CaCu_2O_{6+z}$ (on the left) and $HgBa_2CaCu_3O_{8+z}$ (on the right) (*f*), $Sr_{14}Cu_{24}O_{48}$ (*g*), $Sr_2Cu_3O_5$ (*h*), and $LaCuO_{2.5}$ (*i*).

are characterised by the same type of tetragonal distortion; MnO is isostructural to NaCl. The oxide Mn_5O_8 is described by the formula $Mn_2^{2+}Mn_3^{4+}O_8$. The structure of Mn_5O_8 can be represented by CdI_2-type layers in which 25% of the metal sites are vacant and the Mn^{2+} ions located above and below the vacant positions connect the layers to form a three-dimensional framework.

Depending on the fashion in which the MnO_6 octahedra are joined, tunnels of different shape and size are formed. The presence of tunnels usually leads to high anisotropy of the structure and in some cases to ionic conductivity. For instance, hollandite, cryptomelane, coronadite and α-MnO_2 belong to minerals described by a general formula $A_x(Mn^{4+}, Mn^{3+})_8(O^{2-},OH^-)_{16}$, where A is a large cation, usually, Ba^{2+} (hollandite) or K^+ (cryptomelane). The structure of hollandite comprises double chains of edge-sharing MnO_6 octahedra, which results in the formation of 2×2 tunnels. The structure of psylomelane, $(Ba,H_2O)_2Mn_5O_{10}$, is built of doubled and tripled chains of octahedra and large 2×3 tunnels filled with Ba^{2+} ions and water molecules. Dehydration of this compound by heating to

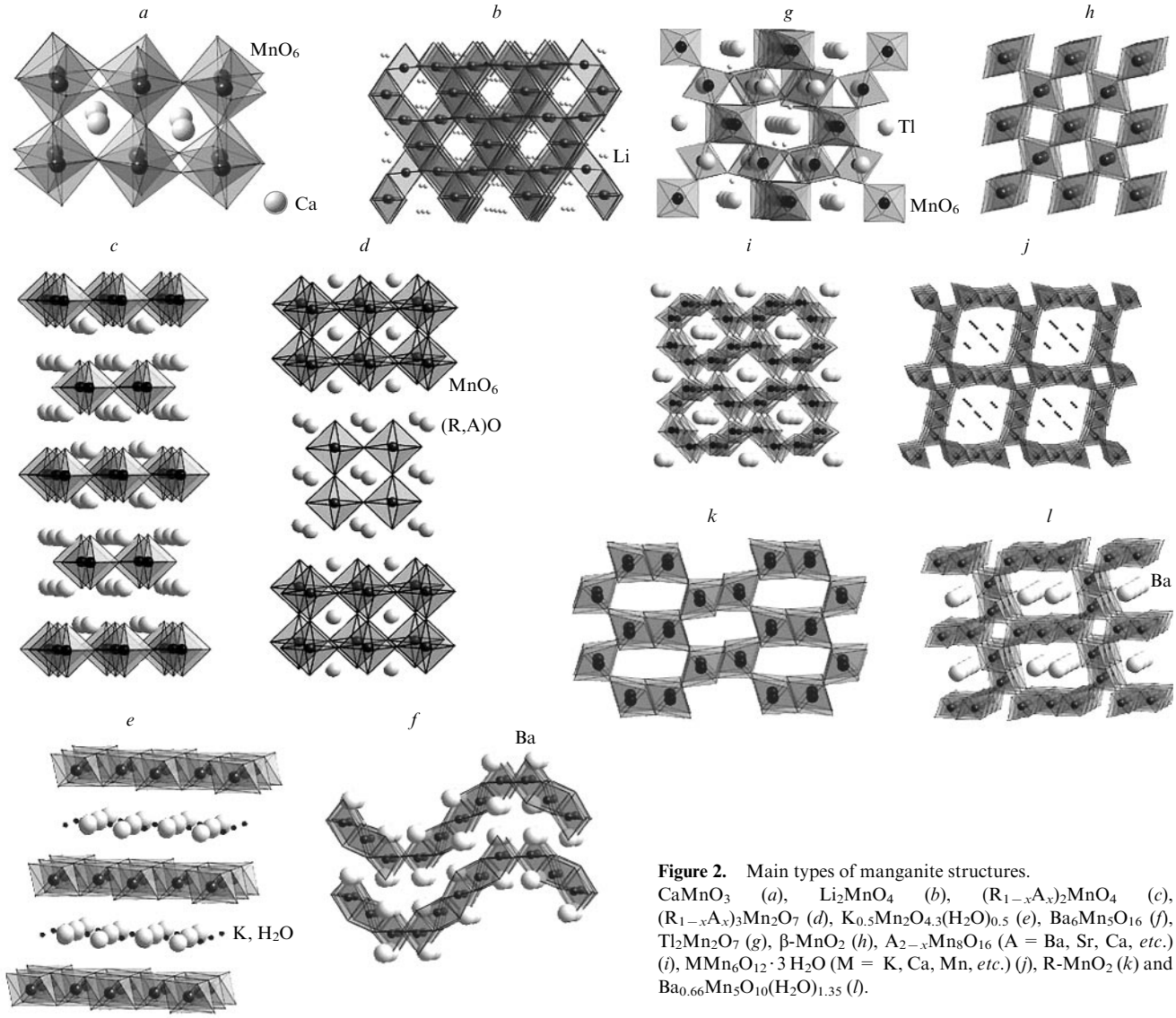


Figure 2. Main types of manganite structures. $CaMnO_3$ (*a*), Li_2MnO_4 (*b*), $(R_{1-x}A_x)_2MnO_4$ (*c*), $(R_{1-x}A_x)_3Mn_2O_7$ (*d*), $K_{0.5}Mn_2O_{4.3}(H_2O)_{0.5}$ (*e*), $Ba_6Mn_5O_{16}$ (*f*), $Tl_2Mn_2O_7$ (*g*), β-MnO_2 (*h*), $A_{2-x}Mn_8O_{16}$ (A = Ba, Sr, Ca, *etc.*) (*i*), $MMn_6O_{12}\cdot 3\,H_2O$ (M = K, Ca, Mn, *etc.*) (*j*), R-MnO_2 (*k*) and $Ba_{0.66}Mn_5O_{10}(H_2O)_{1.35}$ (*l*).

~550 °C is followed by its transformation in hollandite [12] with a disordered structure, which is due to the fact that the large tunnels enclosed on four sides by chains or ribbons of the manganese–oxygen octahedra are partially filled with cations. Tunnels in the todorokite structure are built of tripled 3 × 3 chains of edge-sharing octahedra and contain different numbers of Na, Ca and K atoms; tunnels of more complex shape can also form.[12]

The structure of birnessite, δ-MnO_2, is built of layers comprised of edge-sharing MnO_6 octahedra separated by layers containing water molecules and OH groups (see Fig. 2 *e*). The main structural feature of the manganites $BaMn_3O_5(OH)$ and $BaMn_2O_3(OH)_2$ are ribbons composed of four parallel chains of MnO_6 octahedra.[112] Layered manganites $Ba_4Mn_3O_{10}$ and $Ba_6Mn_5O_{16}$ containing no water molecules are also known.[113] Barium ions stabilise Mn(IV) in the structure. All compounds mentioned above can be obtained *via* 'molecular templates' in the synthesis of manganese oxides and their derivatives by 'soft chemistry' methods (see note ‡).[12]

‡ Here, the term 'soft chemistry methods' covers thermal decomposition of salt and hydroxide components, sol–gel technique, cryochemical or hydrothermal synthesis, which permit fabrication of materials with preset granulometric composition, stoichiometry, *etc.*, at rather low temperatures.

Compounds with a perovskite structure form a broad class of practically valuable materials. Distortion of an ideal perovskite structure in manganites appears due to three factors, namely, cooperative rotation of octahedra about a certain axis, Jahn–Teller distortion of MnO_6 octahedra and displacement of cations from their positions.[2] Thus, the initially cubic perovskite structure can experience a tetragonal, orthorhombic, rhombohedral or monoclinic distortion.

Phases of compositions $A_2Mn_2O_7$ (A = Dy–Lu, Sc, In, Tl) with pyrochlore-type structures [114] have cubic face-centred unit cells. Their structures represent frameworks built of vertex-sharing MnO_6 octahedra with the Mn–O–Mn angle of about 135°. In the structures of $A_2Mn_2O_7$ compounds the atoms A occupy centres of the hexagonal rings formed by the oxygen atoms (O) of MnO_6 octahedra and the oxygen atoms (O′) located above and below the ring plane (see Fig. 2 *g*). Thus, the environment of the atom A can be represented by a distorted cube. The MnO_6 octahedra are distorted, being in fact a kind of trigonal antiprisms; however, this is not a Jahn–Teller distortion characteristic of $R_{1-x}A_xMnO_3$ compounds.

Compounds $(R_{1-x}A_x)_{n+1}Mn_nO_{3n+1}$ belong to the Ruddlesden–Popper phases,[115] *i.e.*, layered manganites with a coherent intergrowth structure of perovskite-type units (the number of layers in the perovskite unit is *n*) and NaCl-type blocks (see

Fig. 2 *e*, *f*). The limiting case $n = \infty$ corresponds to the perovskite structure; the case $n = 1$ corresponds to the K_2NiF_4 structure.

III. Local structure and defects

The possibility of fabrication of cuprate- and manganite-based materials with preset functional properties and solution to the problem of 'anomalous' states of the phases with irreproducible fluctuations of functional properties [116–122] are to a great extent related to control of the cation ordering in the crystal lattices of solid solutions (Fig. 3).

Detailed studies showed that the physical properties of HTSC phases are often governed by the prehistory of samples.[116, 120, 121, 123–125] For instance, $Nd_{1+x}Ba_{2-x}Cu_3O_y$ solid solutions synthesised at low temperatures are characterised by cation disordering; therefore, the degree of local structural distortions in mixed REE–barium cuprates can be controlled by varying the temperature and duration of isothermal annealing (see Fig. 3 *a*). To establish an optimum regime of fabrication of superconducting materials, one should construct TTT-diagrams for different states of solid solutions, *viz*., ceramics, single crystals and films. This approach can also be used for efficient control of solid-phase decomposition of HTSC-cuprates, which can lead to the formation of microinclusions (efficient pinning centres).

Difficulties in studies of cation disordering using diffraction techniques (in particular, X-ray powder diffraction) are associated with integral character of information obtained in the experiments; in this case, investigations of local structural distortions by other methods can be more informative. To perform quantitative analysis of the local structure of high-temperature superconductors and manganites, it is appropriate to employ not only transmission electron microscopy but also efficient methods based on anomalous absorption of radiation, in particular, Mössbauer spectroscopy [119–122] and X-ray spectroscopic analysis [Extended X-ray Absorption Fine Structure (EXAFS)[116, 117]]. The EXAFS technique permits reliable determination of the average distances, coordination numbers and degree of disordering of the coordination environment in different clusters in solid solutions. Valuable additional information suitable for estimation of parameters of the nearest oxygen environment and the valent state of the probe atoms (^{57}Fe, *etc*.) can be extracted from the Mössbauer spectra. Raman spectroscopy provides important information on the local symmetry and force constants of the metal–oxygen bonds.[116, 117] Using Raman spectroscopy and Mössbauer spectroscopy, it is possible to study disordering of light atoms (*e.g*., oxygen atoms), thus complementing information obtained by powder X-ray diffraction methods in structure refinements.

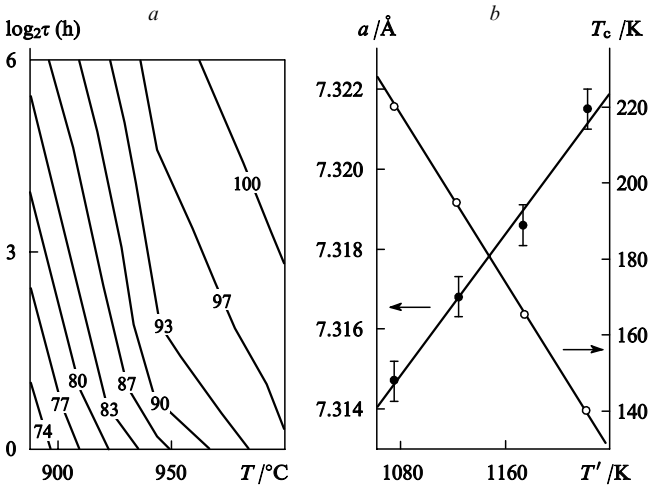


Figure 3. TTT-diagram § for the HTSC phase of $NdBa_2Ca_3O_7$ (*a*) and the lattice parameters and the temperature of magnetic ordering (T_c) of cupromanganite $CaCuMn_6O_{12}$ samples plotted *vs*. synthesis temperature (T') (*b*). Shown in the isolines are the superconducting transition temperatures (in per cent with respect to $T_c = 94$ K).

§ The Time–Temperature–Transformation diagram.

Mössbauer spectroscopy belongs to the most efficient and widely used methods of investigation of the local structure of HTSC phases.[126] The technique precludes on-site studies of defectivenes of the cation sublattice because parameters of hyperfine interactions depend mainly on the state of the first coordination sphere (oxygen environment) of the iron probe atoms occupying positions of copper atoms. At the same time the character of distortions of the oxygen polyhedra surrounding copper atoms is to a great extent governed by the extent of occupation of barium positions by other cations (*e.g*., neodymium ions in the $Nd_{1+x}Ba_{2-x}Cu_3O_z$ solid solution [5]). Schemes presented in Fig. 4 are convenient for establishment of correspondence between parameters of Mössbauer spectra and particular types of coordination polyhedra of the iron atoms occupying positions of copper atoms.[119, 120]

With heterovalent substitution of neodymium for barium the isomer shifts of the corresponding components increase (see Fig. 4) owing to stabilisation of the Fe^{3+} ions occupying the Cu1 positions in the substitutional solid solutions characterised by charge transfer between the dielectric block and the superconducting planes. An increase in the quadrupole splitting of spectral doublets is due to displacement of the apical oxygen O3, which is also characteristic of substitutional solid solutions. A spectral component associated with the $Fe_{Cu1}(III)O_{3+1}$ polyhedron, an unusual distorted configuration of the oxygen environment of the Fe atom occupying the Cu1 position [2 O(*a*) + O(*n*) + O*, see Fig. 1] should be pointed out. This component is characteristic [119, 127] only of annealed samples of the Nd213 : Fe solid solution with superstructural ordering of neodymium and barium atoms.

The main feature of the Mössbauer spectra of the pseudocubic phase $Nd_{1+x}Ba_{2-x}Cu_3O_z$ and substitutional solid solution Nd336 is the presence of components associated to the $Fe(IV)_{Cu1}O_6$ polyhedron.[116–120] These components originate from replacement of neodymium atoms by barium atoms.[118, 119] The $Fe(IV)_{Cu1}O_6$ octahedra are distorted owing to asymmetry of the second coordination sphere comprised of Ba atoms occupying their proper positions and Nd atoms occupying positions of Ba atoms. An increase in the formal oxidation state of iron atoms (decrease in isomer shift) can be explained by the formation of an associate of defects, $Fe(IV)_{Cu1}O_6-Nd_{Ba}$ (Fig. 5). In this case heterovalent substitution of Nd^{3+} for Ba^{2+} leads to displacement of apical oxygen atoms and occupation of vacant oxygen (O4) positions; as a consequence, the coordination sphere of the iron atoms occupying the Cu1 positions takes the shape of a distorted octahedron. No transfer of the excess local positive charge to the $Cu2O_2$ plane occurs, which increases the effective charge on the ^{57}Fe probe atoms. These data confirm the hypothesis that partial exchange of neodymium and barium in their proper crystallographic positions is possible in the pseudocubic phase $NdBa_2Cu_3O_7$ (see Fig. 5 *a*).

At high temperatures, the experimental temperature dependences of the magnetic susceptibility of the CMR manganites $CaCu_xMn_{7-x}O_{12}$ with $x > 0$ obey the Curie–Weiss law. However, the plots show clearly seen downward curvature typical of ferrimagnetics over a broad temperature interval.[16–20] The parameter of the cubic unit cell and the magnetic ordering temperature of the single-phase samples with identical cation and anion compositions depend on the synthesis temperature (see Fig. 3).

These correlations are due to specific structural features of solid solutions. For instance, the $CaCu_xMn_{7-x}O_{12}$ solid solution

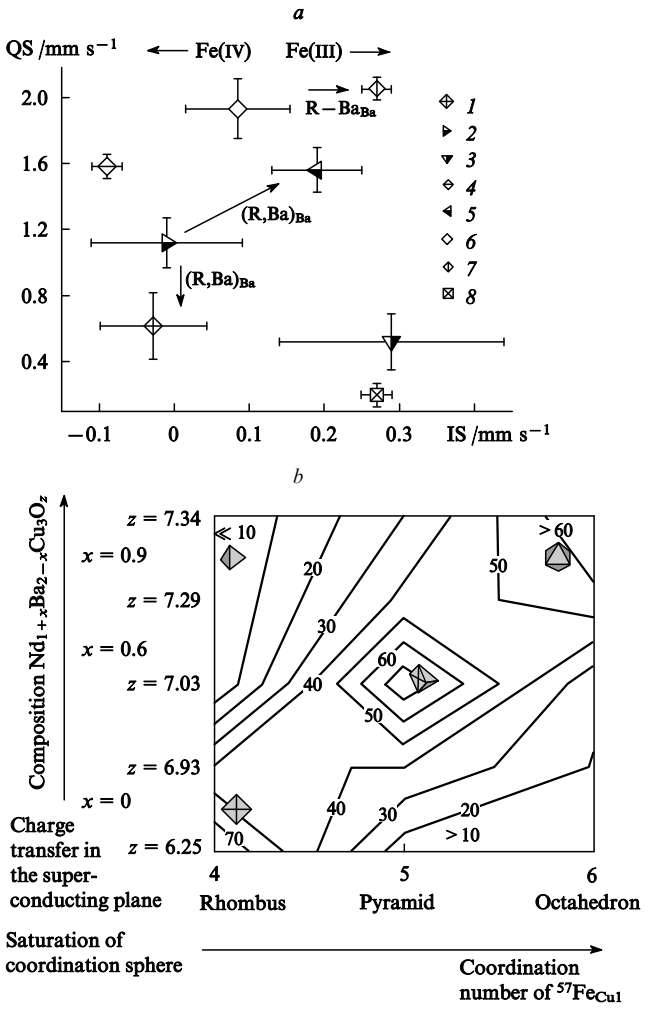


Figure 4. Schematic illustration of the results of Mössbauer spectroscopy studies of mixed REE–barium cuprates (*a*) and a generalised scheme of changes in the iron–oxygen polyhedra (a square, distorted rhombus, pyramid or octahedron) in the Cu1 position in the solid solution phase $Nd_{1+x}Ba_{2-x}Cu_3O_z$ with increasing x and z upon oxidation of samples (*b*). (*a*) Distorted octahedron (Cu1) (*1*), pyramid (Cu1) (*2*), pyramid (Cu2) (*3*), tetrahedron, twins (Cu1) (*4*), distorted pyramid (Cu1) (*5*), rhombus (Cu1) (*6*), distorted rhombus (Cu1) (*7*), and octahedron (Cu1) (*8*); QS is the quadrupole splitting and IS is the isomer shift; shown in the isolines are the contributions of the corresponding coordination numbers of the probe iron atoms (in per cent) (*b*).

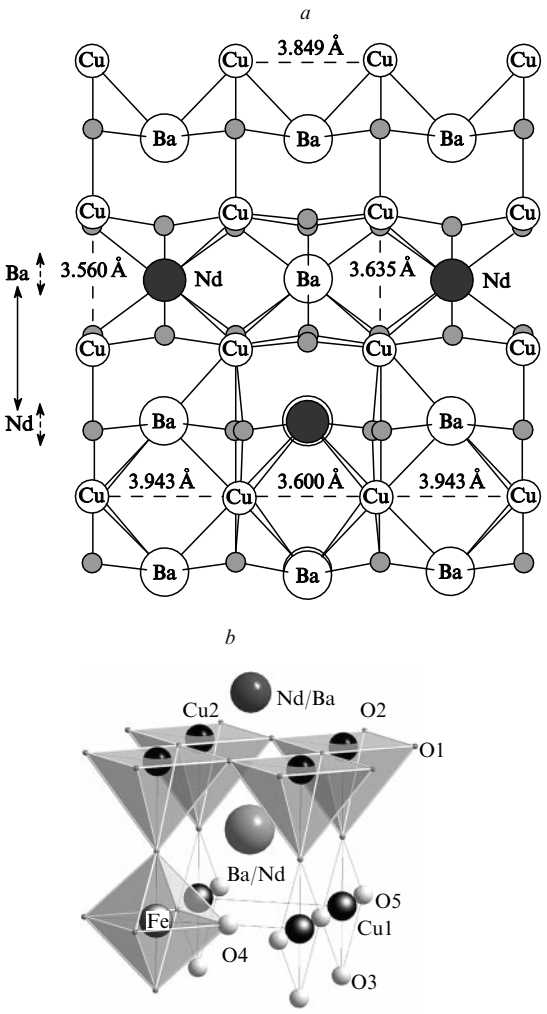


Figure 5. General model of defect (*a*) and a model of associated defects (*b*) $Fe(IV)_{Cu1}O_6-Nd^{3+}_{Ba^{2+}}$, which forms upon doping the substitutional solid solution $Nd_{1+x}Ba_{2-x}Cu_3O_z$ with iron in the case of antistructural disordering of neodymium and barium.

(Fig. 6 *a*) belongs to perovskite-type compounds [16–18] of general formula $AC_3B_4O_{12}$ (A is an alkali metal, alkaline-earth metal or REE cation; B = Mn^{4+}, Mn^{3+}, Ti^{4+}, Ru^{4+} or Ge^{4+}; C = Cu^{2+} or Mn^{3+}). In their framework structures, tunnels are filled with Ca^{2+}, Mn^{3+} and Cu^{2+} cations. The Mn^{3+} ions are also constituents of distorted MnO_6 octahedra occupying the unit cell vertices while the Mn^{4+} cations occupy ideal octahedral positions.

The solid solution (except for the composition with $x = 0$) crystallises in the cubic system (space group $Im\bar{3}$). This is accompanied by doubling of the parameter of ideal perovskite unit cell. The oxidation state of manganese in the B-position depends on the Cu^{2+}/Mn^{3+} ratio (x value) in the solid solution. Magnetic ordering arises as a result of interaction between the Cu^{2+} and Mn^{3+} magnetic sublattices, which depends on the occupation of crystallographic positions by cations and is governed by the procedure employed for sample preparation.

Yet another phase whose properties depend on the sample prehistory is $Ba_6Mn_{24}O_{48}$ with a composite structure (see Fig. 6 *b*) related to the known rutile and hollandite structures.[128] The crystal structure of $Ba_6Mn_{24}O_{48}$ can be represented as a combination of two sublattices, *viz*., a $[Mn_{24}O_{48}]$ framework containing randomly distributed Mn(IV) and Mn(III) and a sublattice of Ba^{2+} chains located within tunnels of the manganese–oxygen framework. Both sublattices have a tetragonal symmetry and the following parameters: $a \approx 18.2$ and $c \approx 2.8$ Å for Mn and $a \approx 18.2$ and $c \approx 4.6$ Å for Ba. The manganese sublattice comprises double columns of edge-sharing $Mn3O_6$ and $Mn1O_6$

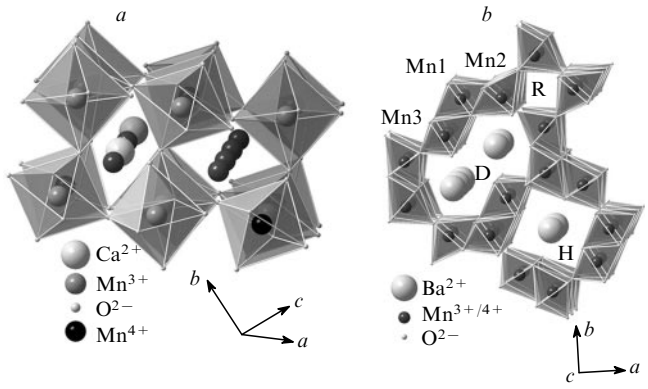


Figure 6. Fragments of the crystal structures of manganites $CaMn_7O_{12}$ (*a*) and $Ba_6Mn_{24}O_{48}$ (*b*).

octahedra and single columns of $Mn2O_6$ octahedra that join the double columns. This results in the formation of double (D), hollandite-type (H) or rutile-type (R) tunnels. Barium cations in the Ba sublattice are partially disordered and can be displaced along the z axis. In addition, barium cations located in the D-type tunnels form domains with a characteristic size of a few nanometres.

The Mössbauer spectra of $CaMn_{6.86}Fe_{0.14}O_{12}$ recorded at 300 K are superpositions of two doublets with similar chemical shifts;[122] small quadrupole splittings of both components confirm that all Fe probe atoms occupy octahedral positions. The Mössbauer spectrum of $Ba_6Mn_{23.76}Fe_{0.24}O_{48}$ is more complicated and can be described as a superposition of four doublets with different quadrupole splittings and equal contributions.

Because the Fe probe atoms have the same oxidation state (+3), both types of the Mössbauer spectra of manganites can be described using a model of continuous distribution of the electric field gradient, P (Fig. 7).[122] A symmetric narrow distribution obtained for $CaMn_7O_{12}$ indicates that the Fe^{3+} cations occupy positions with similar quadrupole splittings and have nearly identical nearest environments. In contrast to the flexible, readily deformable $CaMn_7O_{12}$ framework comprised of vertex-sharing octahedra, the octahedra in the $Mn1O_6-Mn3O_6$ unit of $Ba_6Mn_{24}O_{48}$, which confine the D- and H-type tunnels, are joined rigidly; as a result, distortions typical of these units are imposed on the probe atoms.

The composite structure of $Ba_6Mn_{24}O_{48}$ and the charge redistribution due to specific features of the distribution of barium cations lead to additional local distortions (see Fig.7 *b*).[122] Because of this, the Mössbauer spectrum of $Ba_6Mn_{24}O_{48}$ is best described using the model of continuous distribution of the electric field gradient; the distribution curve exhibits two broadened peaks whose positions correspond to the quadrupole splittings of the ^{57}Fe probe atoms that replace the manganese atoms in the double and single columns. Thus, parameters of spectral components of the Mössbauer spectra are strongly dependent on distortions of polyhedra in the starting structure and are governed by the fashion in which the polyhedra are connected and by the cation distributions within the framework cavities.

Unique information, which can be obtained by analysing the Mössbauer spectra, also concerns some features of the magnetic ordering in these systems. Most of Mössbauer spectroscopy studies of manganites were carried out using $R_{1-x}A_xMnO_3$ phases. The main goal was to investigate their magnetotransport properties as a function of the Mn^{3+}/Mn^{4+} ratio which varied by changing the type and amount of the divalent cation inserted into the perovskite structure.[129–133] Because manganese and iron have similar ionic radii, replacement of Mn^{3+}/Mn^{4+} by Fe^{3+} in the CMR manganites leaves the unit cell parameters almost unchanged but affects the Mn–O–Mn angle, which in turn influences the exchange interaction. Nevertheless, by doping with iron one can obtain information on the localised spin moment in the magnetic ordering region. Establishment of the role of structural distortions in the temperature-induced variations of the magnetotransport properties is also of great importance;[129, 130] therefore, Mössbauer spectroscopy studies allow one to obtain valuable information on specific features of the physical properties of manganites.

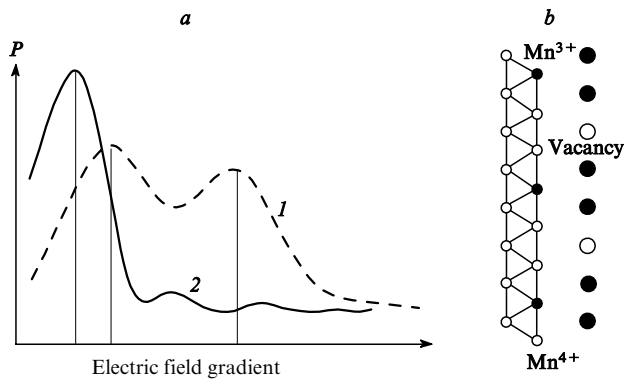


Figure 7. Mössbauer spectra of $Ba_6Mn_{23.76}{}^{57}Fe_{0.24}O_{48}$ (*1*) and $CaMn_{6.86}{}^{57}Fe_{0.14}O_7$ (*2*) samples processed using a model of continuous distribution of electric field gradient (*a*) and a scheme of local changes in the oxidation state of manganese in the case of incomplete filling of tunnels by barium ions (*b*).

IV. Chemical properties and phase diagrams

Difficulties in fabrication of manganite and especially HTSC materials are associated with complex chemical compositions and structures of these compounds (in some cases this is responsible for their thermal and chemical instability). Phase relations in the cuprate and manganite systems depend, in particular, on the size of the cations present in the framework formed by the manganese–oxygen or copper–oxygen polyhedra and on the existence of solid solutions with heterovalent substitution (Figs 8–10).

The $CaMn_2O_4-MnO_x$ polythermal section of the system Ca–Mn–O is characterised by the presence of a large number of phases with different $CaO:MnO_x$ ratios (1:2, 1:3, 1:7 and 1:8; adapted using the data taken from Ref. 134). It was shown [135] that the phase relations in the $BaO-MnO_x$ system are strongly different from those found in the $CaO-MnO_x$ system and the existence regions of compound $Ba_6Mn_{24}O_{48}$ and hollandite $Ba_{2-x}Mn_8O_{16}$ were also determined (see Fig. 8). Thus, changes in the ionic radii of alkaline-earth metal cations (Ca^{2+} or Ba^{2+}) lead to significant changes in the phase relations.

A scheme of phase relations for the polythermal section $CaMn_7O_{12}-CaCu_3Mn_4O_{12}$ of the system Ca–Mn–Cu–O is shown in Fig. 9.[20] The solid solution $CaCu_xMn_{7-x}O_{12}$ with a different degree of substitution ($0 \leqslant x \leqslant 1.5$) is formed in the temperature interval $750 \leqslant T \leqslant 1060$ °C. The highest degree of substitution ($x = 1.5$) is achieved at ~850 °C, whereas the $CaCuMn_6O_{12}$ phase ($x = 1$) exists in a broad temperature range from 750 to 1000 °C. At ~1060 °C, the complex oxide $CaMn_7O_{12}$ decomposes into marokite $CaMn_2O_4$ and hausmannite Mn_3O_4. At 750–1050 °C, the $CaCu_xMn_{7-x}O_{12}$ solid solution with the maximum degree of substitution is in equilibrium with $CuMn_2O_4$ and CuO.

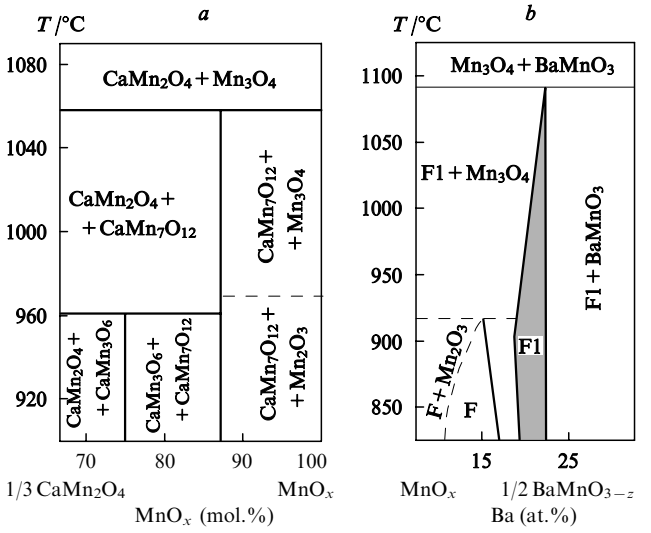


Figure 8. Polythermal section $CaMn_2O_4-MnO_x$ (*a*) and a scheme of phase relations in the system Ba–Mn–O (*b*).
$p_{O_2} = 1$ (*a*) and 0.21 atm (*b*).

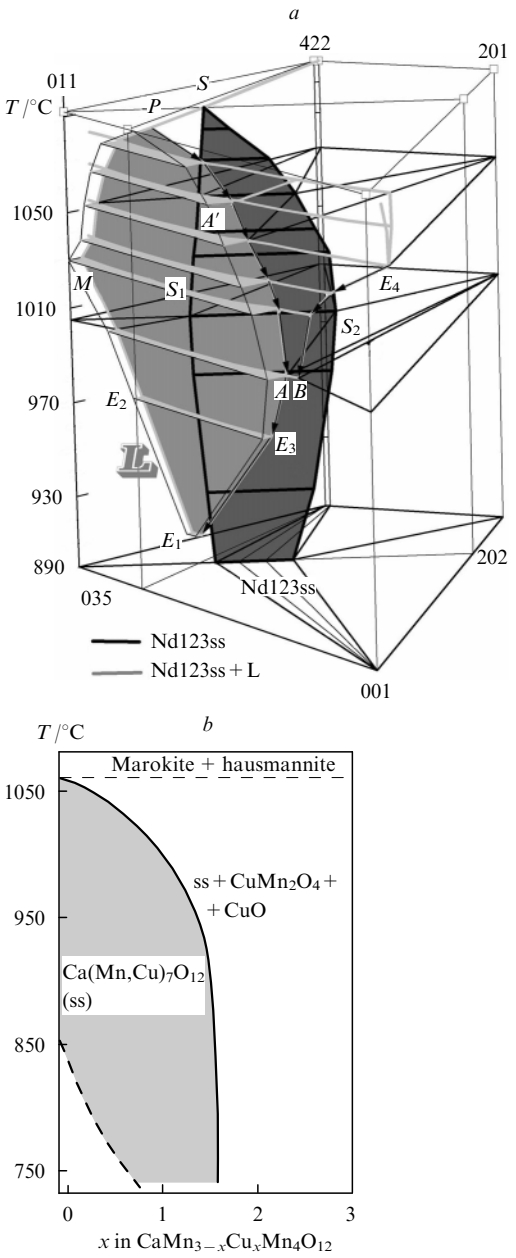


Figure 9. Three-dimensional model for phase relations in the $NdO_{1.5}$–BaO–CuO_x system at $p_{O_2} = 0.21$ atm (*a*) and a scheme of $CaMn_7O_{12}$–$CaCu_3Mn_4O_{12}$ polythermal section at $p_{O_2} = 1$ atm (*b*). The region of the $Nd_{1+x}Ba_{2-x}Cu_3O_z$ solid solution (S_1SS_2 is the high-temperature bound of the stability region) is shown by dark grey and the fraction of the liquid surface, which is in equilibrium with the solid solution phase ($E_1E_2MPA'AE_3$), is shown in light grey. Connodes for the two-phase region (solid solution – melt) are not shown. A and B are the points of peritectic decomposition of the limiting solid solution (Nd123ss + Nd_2CuO_4 + L) and the Nd_2CuO_4–CuO–(BaO) eutectic, the point A′ corresponds to passage from the equilibrium Nd123ss + 201 + L to the equilibrium Nd123ss + 422 + L; E_1, E_4 are eutectics in the binary systems $BaCuO_2$–CuO and Nd_2CuO_4–CuO, respectively.

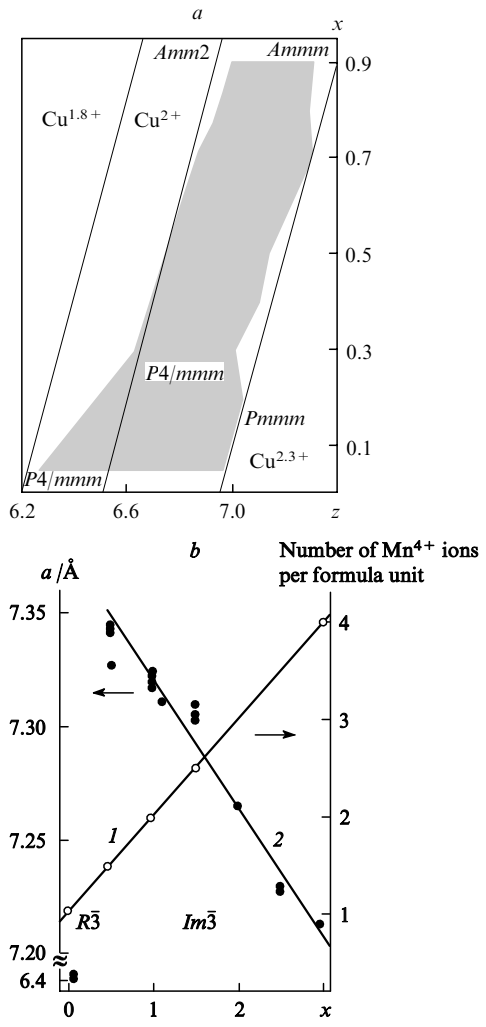


Figure 10. Average oxidation states of copper as functions of the cation and anion compositions of the $Nd_{1+x}Ba_{2-x}Cu_3O_z$ solid solution (*a*); dependences of the average oxidation state of manganese in the $CaCu_xMn_{7-x}O_{12}$ solid solution upon replacement of Mn^{3+} by Cu^{2+} (*1*) and of the lattice parameter (*2*) on *x* (*b*). The region of existence of the solid solution within its cationic and anionic composition ranges is shown in grey. Shown are the space groups of symmetry of the phases.

Phase relations in the supersolidus regions of the systems containing transition elements can be illustrated [4, 5, 136] taking the family of HTSC cuprates $RBa_2Cu_3O_z$ as an example (see Fig. 9). When considering the systems R_2O_3–BaO–CuO_n–O_2, the following deserves particular attention: the partial pressure of oxygen (especially in the coexistence regions of the solid and liquid phases) [137, 138] and the possibility of formation of substitutional solid solutions in which barium atoms are replaced by REE atoms due to rather large ionic radii of the early REE (La, Pr, Nd, Sm, Eu, Gd). For instance, the existence region of the solid solution $Nd_{1+x}Ba_{2-x}Cu_3O_z$ has a 'classical shape' and the limiting phases of compositions 123 and 213, $-0.1 < x < 1.0$ (see Fig. 9 *a*), are characterised by peritectic melting and a maximum decomposition temperature [5, 136] achieved at $x \approx 0.1$. Equilibria with the liquid phase in the solid solution – melt region and reasons for changes in the types of secondary phases ($Nd_4Ba_2Cu_2O_{10}$ and Nd_2CuO_4) formed in the course of peritectic decomposition have been studied in detail. [4, 136–140]

A good example of thoroughly studied materials with a broad region of cation and anion homogeneity is provided by HTSC cuprates (see Fig. 10 *a*). The existence region of solid solutions can be divided into three regions. [4, 136, 137, 141] Compounds with $0 < x < 0.3$ have tetragonal unit cells after quenching and orthorhombic unit cells after oxygenation, the unit cell constants *a* and $c/3$ ($a < c/3$) monotonically decrease as Ba^{2+} ions are replaced by ions with smaller radius (Nd^{3+}). At $0.3 < x < 0.6$, the unit cell is always tetragonal irrespective of the oxygen content ($a \approx c/3$). At $0.6 < x < 0.9$, the phase has an orthorhombic unit cell due to superstructural ordering of neodymium and barium ions. Interrelation between the cation and anion ordering was confirmed by the T–x–z-diagrams. [137] The range of the average oxidation

states of copper in the solid solution varies in accord with the concentration phase transitions; the lower the degree of substitution, the broader the range (see Fig. 10 *a*).

In the $Ca(Mn,Cu)_7O_{12}$ solid solution an increase in the degree of substitution of copper(II) for manganese(III) causes a reduction of the upper bound of the stability region of the solid solution from 1060 to ~950 °C (see Fig. 9 *b*) due to an increase[20] in the Mn^{4+} content (see Fig. 10 *b*). The lattice constant of the cubic solid solution (space group $Im\bar{3}$) decreases obeying the Vegard law (see Fig. 10 *b*). This is consistent with the heterovalent substitution of Mn^{3+} ions for Cu^{2+} ions, which causes an increase in the Mn^{4+} content in the phase and, hence, a decrease in size and in degree of distortion of the manganese–oxygen framework. Thus, the oxidation states of copper and manganese play the key role in stabilities of cuprate and manganite phases.

V. Single crystals

Construction of phase diagrams is an important stage in experimental studies of the growth of single crystals. Cuprate and manganite single crystals with preset chemical homogeneity, size, shape, concentrations of defects and impurities (Figs 11 and 12) are necessary for both basic and applied research and, in particular, for studies on crystallisation mechanisms of multicomponent melts. The advantage of these single crystals is the possibility of investigating the anisotropy of properties on different crystal faces. This is widely used in structural analysis, spectroscopy, oxygen diffusion studies, atomic force microscopy, in the determination of fundamental physical constants,[4] *etc*.

Single crystals of HTSC materials were obtained using almost all known melt growth techniques modified to allow for specific features of HTSC:[4, 138, 142–147] spontaneous crystallisation from solution in melt, Bridgman method, zone melting and the Kyropulos and Czochralski methods (see Fig. 11). Distinctive features of most of them are multicomponent composition of crystallising systems and a variety of interfacial interactions.[4] The mechanisms of crystallisation and growth of faces of HTSC crystals in different crystallographic directions seem not to be specific to the systems in question, being also different for each method mentioned above. The most commonly encountered growth mechanisms are the Frank–Kabrer mechanism and layer-by-layer growth.[4]

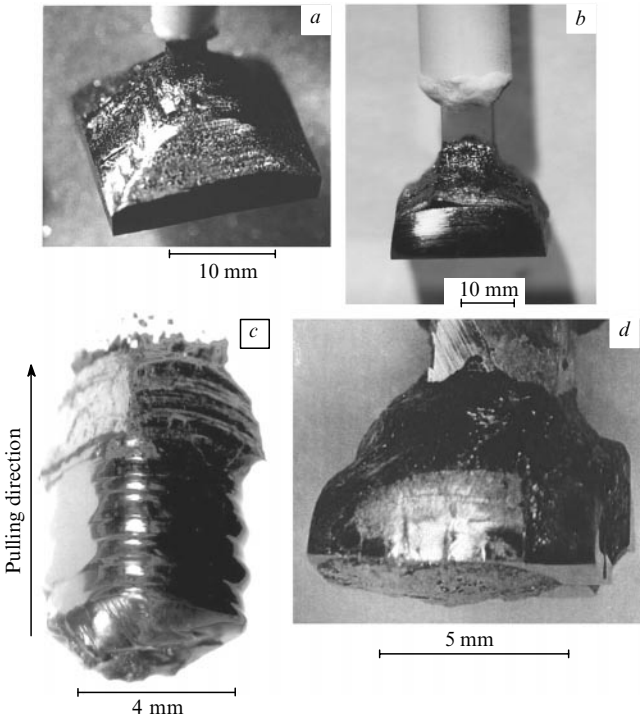


Figure 11. Photographs of the crystals of mixed REE–barium cuprates of different compositions grown using the modified Czochralski method (courtesy of Prof. Y Shiohara, SRL ISTEC, Japan).[142–145] One of the largest superconducting $NdBa_2Cu_3O_7$ crystals (*a*); large superconducting $YBa_2Cu_3O_7$ crystal grown using the modified Czochralski method (*b*); a cylindrical crystal of the superconducting phase $YBa_2Cu_3O_7$ grown in an automated growth setup (*c*); and a $Nd_{1.85}Ba_{1.15}Cu_3O_7$ crystal possessing a semiconductor-type temperature dependence of resistance (*d*).

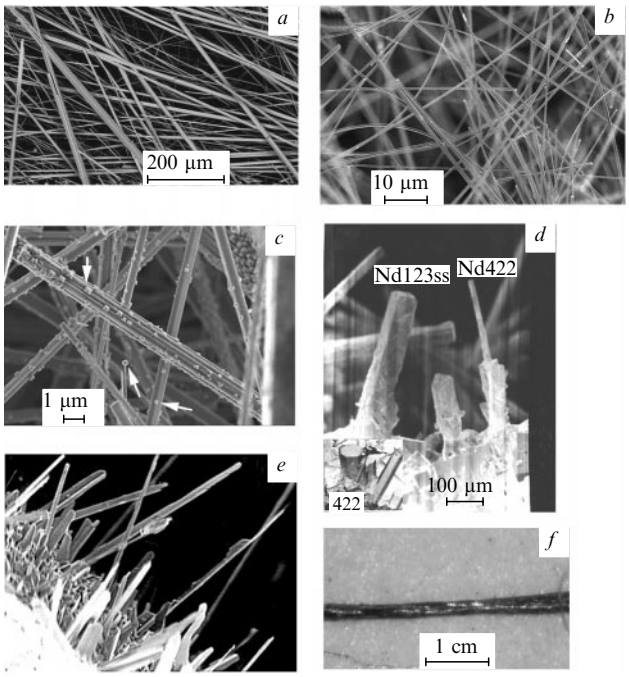


Figure 12. Micrographs of cuprate and manganite whiskers.
Hollow hollandite whiskers ($Ba_{2-x}Mn_8O_{16}$) obtained by isothermal evaporation of chloride fluxes (*a*); $Ba_6Mn_{24}O_{48}$ whiskers with a tunnel structure oriented along the growth direction, obtained by isothermal evaporation of KCl (*b*); the same crystals after storage in molten $LiNO_3$ at 300 °C (ion exchange causes replacement of barium in the channels by lithium; the arrows show octahedral spinel Li_2MnO_4 crystals oriented along the etching pits of the whiskers) (*c*); high-temperature superconducting $Nd_{1+x}Ba_{2-x}Cu_3O_z$ and $Nd_4Ba_2Cu_2O_{10}$ whiskers formed in the polythermal regime; superconducting $Bi_2Sr_2CaCu_2O_8$ whiskers (*e*) and a wire prepared by pulling of the glue mass containing $Ba_6Mn_{24}O_{48}$ filaments (*f*).

Anisotropy of the rate of growth of mixed REE–barium superconducting cuprates along the main crystallographic directions depends on the REE type and on crystallisation conditions in a very complicated manner.[4] This can be due to the crystallographic anisotropy, different energies of crystal faces and different growth mechanisms; the anisotropy of growth also causes changes in the face morphology and crystal habit (see Fig. 11). For instance, crystals grown by spontaneous crystallisation usually have a shape of thin plates with the smallest thickness along the ⟨001⟩ direction, because at high cooling rates ('kinetic control') the growth rate of the {100} faces is nearly five times higher than the growth rate of the {001} faces. A decrease in the melt cooling rate down to 0.5–1.0 deg h^{-1} causes the formation of thick prisms-parallelepipeds and even isometric crystals. Under these conditions not only the {100}, {010} and {001} faces but also the {101}, {011} and {111} faces grow, *i.e*., the crystal grows under thermodynamic control.

The method of top-seeded crystal pulling from a supercooled melt is characterised by rather low supersaturations; here, an important role is played by the hydrodynamic conditions and the temperature and concentration distributions near the growing crystal.[142, 143] By controlling the pulling rates and growth aniso-

tropy it is possible to grow various 'bulk' single crystals including pyramidal crystals with extending base, large isometric crystals with small edge angularity, pyramidal crystals with 'concave' low face and cylindrical crystals (see Fig. 11). Other crystallisation techniques allow growth of single crystals in the form of needles, plates and parallelepipeds.[4,5]

Considerable advances have been made in the field of single-crystal growth due to the development of a method of continuous growth of mixed REE–barium cuprate crystals,[142] in which the growing single crystal is fed under steady-state conditions owing to separation of the crystal growth zone ($T < T_p$) and the Y_2BaCuO_5 dissolution zone ($T > T_p$, T_p is the peritectic temperature) by a melt layer. In the presence of a temperature gradient (~ 3 deg cm^{-1}), diffusion and convective transport of yttrium-saturated melt occurs across this layer. To prevent the crystal contamination with the crucible material, crucibles made of yttria (generally, an REE oxide) are often used. Growth of Nd123 single crystals by the modified Czochralski method is performed in the presence of small temperature gradient.[143,144] Because of much higher solubility of neodymium oxide in the melt here we deal with isothermal crystal growth from supercooled melt in a crucible made of neodymium oxide. The modified Czochralski method is versatile and allows one to grow single crystals of almost all R123 (R = Y, Nd, Sm, Pr) phases and $(R^1R^2)Ba_2Cu_3O_z$ (R^1 = Y, R^2 = Sm, Nd), $Nd_{1+x}Ba_{2-x}Cu_3O_z$, $Pr_{1+x}Ba_{2-x}Cu_3O_z$, $Nd_{1+x}Ba_{2-x}Cu_{3-y}Ga_yO_z$, $YBa_2Cu_{3-y}Zn_yO_z$, *etc.*, solid solutions.[4,143] Using the floating zone technique, superconducting Pr123 crystals were obtained at reduced partial pressure of oxygen.[148] Recently, considerable attention has been paid to the development of methods of preparation of single-crystalline HTSC 'whiskers' (see Fig. 12).[149–152] These crystals can possess unique electrophysical and mechanical properties.

Experimental difficulties in growing manganite single crystals are caused by high melting temperatures of these compounds (~ 2000 °C) and low solubility in conventional high-temperature solvents. In most cases this problem is solved using an IR heated floating zone technique[153] because it excludes the interaction between the crystal and the container material. To grow manganite crystals, it is necessary that the feed rod have the same density along the whole length and homogeneous composition. The feed rods are produced by hot pressing and sintering appropriate components at ~ 1100 °C. This allows one to avoid melt penetration into pores of the sample (due to the capillary effect) and to stabilise the melt composition in the growth zone. The seeds used are both dense polycrystalline samples and pre-oriented single crystals. For instance, $La_{1-x}A_xMnO_3$ (A = Sr, Ca; $x = 0-0.3$), $Nd_{0.7}Sr_{0.3}MnO_3$, $La_{0.5}Ca_{0.5}MnO_3$ and $Nd_{1-x}(Sr,Pb)_xMnO_3$ rods (crystals) nearly 5 mm in diameter are usually grown at a growth zone rate of 5 to 7 mm h^{-1}. The floating zone method is also efficient for growth of single crystals of the Ruddlesden–Popper phases[154] possessing highly anisotropic properties due to their structural features. At the same time this technique is unsuitable for the synthesis of manganites $R_{1-x}A_xMnO_3$ (A is an alkali metal) owing to high volatility of A_2O oxides and of thermally unstable phases related to pyrolusite MnO_2 and hollandite.

Using traditional spontaneous crystallisation technique, it is possible to grow alkaline-earth manganite crystals. For instance, isotropic $Ln_{1-x-y}Sr_xPb_yMnO_3$ (Ln = La, Pr, Nd) crystals with a volume of up to 3 cm^3 are obtained using Bi_2O_3, PbF_2 and PbO as fluxes. $Sr_4Mn_3O_{10}$ crystals were flux grown with $SrCl_2 + SrF_2$.[155] An alternative to spontaneous crystallisation is electrolysis of manganite solutions in a molten mixture of Cs_2MoO_4 and MoO_3 using platinum electrodes in crucibles made of stabilised zirconia.[156] This technique was employed to obtain plate-like, strontium-doped lanthanum manganite crystals with a surface area of 0.25 to 4 mm^2. The temperature of the process was reduced to 1000 °C (alkali metal doped manganite crystals grow at 980–1000 °C).

Often, crystals of metastable or thermally unstable phases, *e.g.*, $BaMnO_3$, $BaMn_2O_3(OH)_2$ and $BaMn_3O_3OH$ are grown using the hydrothermal method.[112,157] This permits preparation of manganites with tunnel structures (pyrolusite, ramsdelite, hollandite and todorokite, see Fig. 2) starting from a layered manganite with the structure of sodium-containing birnessite treated with LiCl, KCl, $MgCl_2$ or $BaCl_2$ solutions; the size and shape of tunnels in the structure depend on the type of the cation inserted.[12]

MnO_2 and Mn_3O_4 nanowires were grown using hydrothermal method or microemulsions.[158,159] A simple method called isothermal evaporation of chloride fluxes was developed[135] to obtain filaments of potentially one-dimensional superionic conductors $BaMn_8O_{16}$ and $Ba_6Mn_{24}O_{48}$ with tunnel structures (see Fig. 12). The method not only provides a means of transportation of the components required for crystal growth by the 'vapour–liquid–crystal' mechanism but also allows an important problem of selection of the crystals obtained from solvent (flux) to be solved. The optimum temperature for growth of $Ba_6Mn_{24}O_{48}$ crystals from KCl is 950 °C. At $T < 900$ °C, an impurity of hollandite whiskers was always observed, while at $T > 950$ °C, hausmannite was formed, which is consistent with the phase diagram (see Fig. 8 *b*). Within the limits of experimental error for local X-ray spectroscopic analysis the crystals obtained were chemically homogeneous along the length and contained less than 1 at.%–2 at.% of flux components (K, Cl). These phases with anisotropic unit cells were also observed in the form of (i) 'pseudo-single-crystalline' whiskers with small-angle boundaries, (ii) hollow needles, (iii) dendrites and (iv) 'bundles' (see Figs 12 *a–c*). The $Ba_6Mn_{24}O_{48}$ whiskers were 1 to 5 μm thick, the hollandite whiskers were somewhat thicker ($\sim 20-50$ μm).

VI. Microstructure and new methods of preparation of ceramic composites

Methods of fabrication of polycrystalline materials with improved functional properties are based on the concept of a real structure characterised by a number of hierarchic levels of organisation.[5] As shown above, the fundamental properties of compounds are determined by the crystal structure and its local distortions. Individual crystallites comprised of certain units separated by extended defects form the mesoscopic level of structural organisation. The macroscopic level is formed by ensembles of crystallites and pores.

Superconducting phases with controllable superconducting transition temperature can be synthesised in a different manner.[5] At the same time improvement of such important characteristics of superconducting materials as the critical current density, J_c, and its stability in high magnetic fields faces reasonable difficulties. The superconducting transition temperatures of HTSC ceramics much exceed those of metallic superconductors while the coherence length of ceramics (0.2 nm) is an order of magnitude smaller than that of intermetallides. The thickness of grain boundaries in polycrystalline HTSC ceramics is greater than the coherence length; therefore, the magnitude of current flowing along the ceramic samples is strongly dependent on the intergrain contacts. In addition, layered crystal structures of almost all high-temperature superconductors cause their physical properties to be highly anisotropic; this requires texturing of polycrystalline materials. High-temperature superconductors are type II superconductors; therefore, under some conditions the external magnetic field can penetrate into the bulk of a sample in the form of Abrikosov vortices trapped in non-superconducting inclusions (pinning centres).[5,160] To achieve high critical current densities (greater than 10^5 A cm^{-2}) and stabilise them in the magnetic fields of 1 to 10 T, one should create efficient pinning centres, which is a practically important problem in the materials science of HTSC.

The magnetoresistance, as the phenomenon of relative change of electrical resistance in an external magnetic field, has long been known.[9–11] Intrinsic magnetoresistive effects are due to the properties of a particular compound; the tunnelling magnetoresistive effects are related to the specific features of interfaces and

various natural or artificial inhomogeneities. A commonly accepted model for the mechanism of intrinsic magnetoresistance involves the concept of double exchange first proposed by Ziner,[161] which has been successfully used to explain the magnetoresistance effect in $R_{1-x}A_xMnO_3$ solid solutions. The experimentally observed magnetoresistance is also explained by the influence of additional factors, in particular, the electron–phonon interaction and dynamic Jahn–Teller effect for Mn^{3+} (see Ref. 162). A model by Millis, Littlewood and Shraiman [163] includes local rearrangement of the crystal lattice, because hopping of charge carriers between the lattice sites occupied by the manganese ions produces a charge fluctuation and the charge carrier in the crystal becomes a charged magnetoelastic polaron.

The model of double exchange is inapplicable to pyrochlore-type manganites and cupromanganites [16–19, 114] because of the absence of the Mn^{3+} ions or large deviation of the Mn–O–Mn angle from 180°. In this connection alternative models for description of the CMR phenomemon have been developed. These are, *e.g.*, the magnetic impurity theory [164] and a model based on the concept of one-electron σ-bonding between the manganese and oxygen ions due to high covalency of the manganese–oxygen bond, which leads to the formation of a strongly correlated electronic state.[165]

The intrinsic magnetoresistance of polycrystalline materials is only a part of the total magnetoresistance. Indeed, in most of these materials the magnetoresistance effect manifests itself in wide temperature and magnetic field ranges rather than near the Curie point in high magnetic fields. In this connection the existence of the tunnelling magnetoresistance was hypothesised.

Peculiarities of the microstructural organisation of polycrystalline materials (see above) make traditional methods of solid-phase synthesis of cuprates and manganites inefficient for fabrication of materials with good operating characteristics. Hence, it was reasonable to elaborate new methods of synthesis of cuprates and manganites, *e.g.*, techniques involving mechanically activated reactants [166] and melt technologies [5, 160] permitting an integrated treatment of the real structure of a material.

A method of fabrication of $RBa_2Cu_3O_z$-based superconducting materials (Fig. 13) at record low temperatures (500–600 °C) during unique short reaction times (10–30 min) was proposed.[166, 167] The starting reactants were [166] copper(I) oxide obtained using 'soft' chemistry methods and a mixed oxide '$YBa_2O_{3.5}$' (containing BaO_2). Both compounds were mechanically activated in a ball mill and then 'warm' pressed at 250 °C. A feature of the technique is the use of oxides as reactants which react without liberation of gaseous products that could break the intergrain contacts in the reaction mixture. In addition, the mixed REE–barium oxide is a source of the yttrium and barium ions with low diffusion mobilities, whereas the copper(I) oxide is a source of the copper ions characterised by higher diffusion coefficients. Different reactants contain different cations; this provides high chemical potential gradients of the components, unambiguous direction of the diffusion processes in the system and, by and large, a high driving force of the formation of a superconductor. Pilot experiments were carried out on fabrication of superconducting aluminum-sheathed tapes with an oxide wire which becomes a superconductor ($T_c \approx 45–85$ K) after low-temperature synthesis at 600 °C using a procedure of mechanical activation of 'two-powder' precursors proposed in Ref. 166.

To prevent reduction of manganese to an oxidation state lower than +3 in the synthesis of a family of manganites, high oxygen pressure is required. For instance, phases in the system Ca–Mn–Cu–O are usually synthesised under oxygen pressures of 0.18–50 000 atm in sealed quartz ampoules or autoclaves.[16–18] The use of mechanically activated reactants, which is similar to that described above for the HTSC phases,[20] appeared to be efficient for the synthesis of cupromanganites. Clearly, pressing of mechanically activated powders at elevated temperatures (250–400 °C) to a great extent promotes a subsequent solid-phase reaction and permits the obtaining of complex manganese oxides

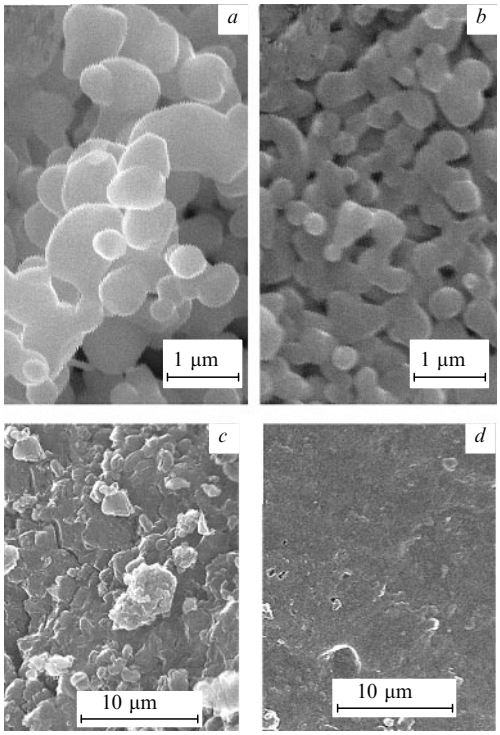


Figure 13. Changes in the morphologies of the ceramic samples of CMR manganites $CaCuMn_6O_{12}$ (*a*, *b*) and HTSC cuprates $YBa_2Cu_3O_z$ (*c*, *d*) obtained using mechanically activated reagents pressed at 250 °C. Duration of mechanical activation of the phases, min: 15 (*a*, *c*) (pressing under different loads), 120 (*b*) and 240 (*d*).

in the form of ceramics (see Figs 13 *a*,*b*) with improved magnetotransport properties at so low temperatures that Mn(IV) appears to be stable at a standard partial pressure of oxygen $p_{O_2} = 0.21–1$ atm.

Microstructural features have a strong effect on the transport properties of HTSC ceramics;[4, 5] this is also characteristic of manganites and cupromanganites. In spite of the fact that the CMR is intrinsic in mixed-valence manganites, a decrease in the grain size can make the role of the grain boundaries more important and favour charge transport due to the spin-polarised intergrain tunnelling. This can provide an explanation for 200% to 300% variation of the magnetoresistance of samples of the same composition $CaCuMn_6O_{12}$, which were synthesised under the same conditions but had different microstructures (Fig. 14).

Melt techniques have provided the best route to HTSC-materials.[4, 5] A feature of the melt-produced, coarse-grained HTSC ceramics is the presence of ensembles of pseudo-single-crystal domains of size 0.5 to 5 cm. Each domain is an aggregate of $RBa_2Cu_3O_z$ lamellae (5–50 nm), which are aligned and separated by small-angle boundaries through which electric current can flow. The microstructure of the melt textured HTSC ceramics is characterised by the presence of different types of extended defects such as twin boundaries, highly disperse inclusions of the non-superconducting phase, dislocations, microcracks and macrocracks.

Thus, melt-produced HTSC ceramics can be considered as a system possessing pronounced 'co-operative' superconducting properties due to specific crystallisation mechanisms. Pseudo-single-crystal domains form macroscopic aggregates capable of carrying heavy currents, because at the microstructural level they represent a system with pure superconducting boundaries and biaxially textured crystallites. High concentration of defects favours the formation of efficient pinning centres.

In addition to coarse-grained ceramics (Fig. 15 *a*) modern methods permit fabrication of HTSC-materials of complex

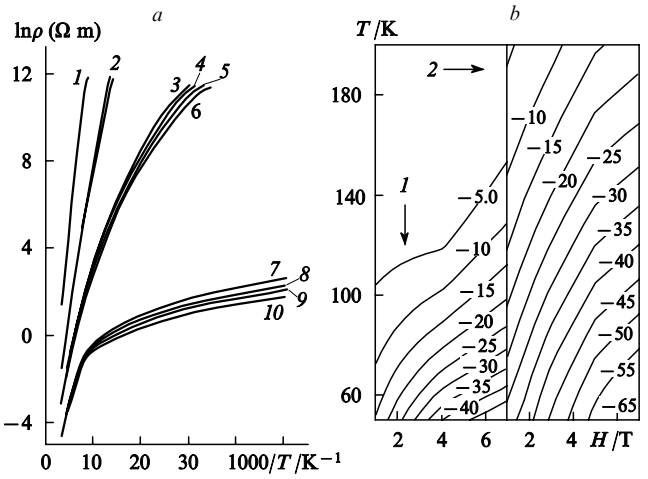


Figure 14. Magnetoresistive properties of the ceramic samples of $CaCu_xMn_{7-x}O_{12}$ solid solutions prepared using mechanically activated reactants (*a*) and the magnetoresistive effect in $CaCuMn_6O_{12}$ samples with different microstructures (*b*).
$x = 0$ (*1*), 0.5 (*2*), 1.0 (*3*–*6*), 1.5 (*7*–*10*); $T_c = 194$ (*1*–*6*) and 245 K (*7*–*10*); $H = 0$ (*3*, *7*), 1 (*4*, *8*), 3 (*5*, *9*) 5 T (*6*, *10*) (*a*); the microstructures of the samples *1* and *2* are shown in Figs 13 *a* and 13 *b*, respectively; figures in the isolines illustrate the magnetoresistive effect in % (*b*).

shape and(or) in the form of thick-film coatings (Figs 15 *b*–*e*).[168–174] These methods include saturation of a fabric obtained from yttria filaments or a ceramic 'foam' prepared using Y_2BaCuO_5 powder, organic binder and a polymer matrix with high-temperature cuprate melt.[168–173] On cooling of the Y_2BaCuO_5–melt system the non-superconducting REE oxides are transformed in the superconducting mixed REE–barium cuprate due to the reaction with the melt. Introduction of oriented seeds initiates directed crystallisation of the superconducting phase in the form of ceramics, fabric, foam, *etc.* (Figs 15 *b*,*c*). Studies on 'glueing' of individual geometrically matched blocks of dense coarse-grained ceramics into complex structures using mixed REE–barium cuprates, silver-containing and fluorine-containing fluxes with low melting temperatures (Fig. 15 *d*)[174] deserve particular attention. A unique method of directed crystallisation of mixed REE–barium cuprates on metallic substrates in artificially induced concentration gradient of the rare-earth elements was developed [175] (Fig. 15 *e*).

The use of the concentration gradients [175] is an efficient method of control of the crystallite orientations in thick films because of large local supersaturations (supercooling) produced in the system. The entire starting film can be in the form of a layer of a vapour deposited Y_2BaCuO_5 phase, which is then saturated with a melt. A seed strip of a polycrystalline $NdBa_2Cu_3O_z$ powder is arranged along the main layer. On the opposite side, an Yb_2BaCuO_5 strip is arranged to increase the concentration gradient and to preclude the formation of the HTSC phase in the adjacent region.

Cooling of the system after saturation with the melt is accompanied by nucleation of crystallites of the HTSC phase near the seed strip. Similarly to seeds, the HTSC crystallites have arbitrary initial orientations and growth directions. The direction in which crystals grow at the highest rate 'survives', *i.e.*, geometrical selection of crystallites occurs. As a result, the spatial evolution of the whole ensemble of crystallites beyond the transient zone of certain length occurs concertedly along the same direction. Experimental confirmation (see Fig. 15 *e*) of the efficiency of thick film texturing using a concentration gradient opens up great prospects for the development of new technologies of fabrication of highly oriented layers of functional materials with anisotropic properties.

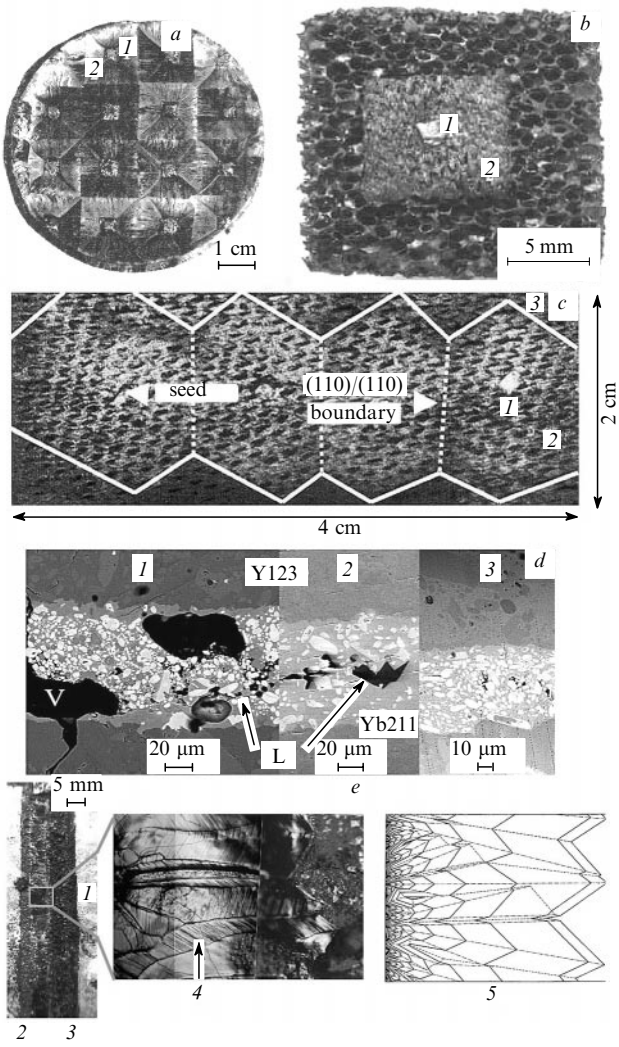


Figure 15. Coarse-grained superconducting samples of melt-solidified mixed REE–barium cuprates (courtesy of Prof. G Schmitz, ACCESS e.V., Germany).
(*a*) $YBa_2Cu_3O_z$ ceramics: mutually oriented $NdBa_2Cu_3O_z$ seed crystals (*1*) and pseudo-single-crystal blocks (*2*); (*b*) superconducting ceramic $YBa_2Cu_3O_z$ 'foam': $NdBa_2Cu_3O_z$ seed crystal (*1*) and pseudo-single-crystal domain (*2*); (*c*) HTSC-samples with a fabric structure obtained by infiltration technique using seeds (*1*), oriented domains (*2*) and a polycrystalline domain (*3*); (*d*) joining of pseudo-single-crystal superconducting mixed REE–barium cuprates using low-melting ytterbium–barium cuprates: polished surfaces of $YBa_2Cu_3O_z$ blocks (*1*); the same with an external pressure of 20 kPa applied (*2*); the same with PtO_2 added to reduce the size of crystallites of the secondary phases (V are structural voids and L is the liquid phase) (*3*); (*e*) spontaneous directed crystallisation in the presence of concentration gradient: substrate (silver–palladium alloy) (*1*); a seed strip of polycrystalline $NdBa_2Cu_3O_z$ with high temperature of peritectic melting, obtained by screen printing (*2*) and an $YbBa_2Cu_3O_z$ or Yb_2BaCuO_5 strip to induce the concentration gradient of the rare-earth element. The rectangle indicates a region of the Y_2BaCuO_5 layer impregnated with the cuprate melt in which crystallites of the superconducting $(Y,Nd,Yb)Ba_2Cu_3O_z$ solution grow on cooling (*3*), general view of superconducting crystallites at higher magnification (*4*) and graphic reconstruction of the grain selection process (*5*).

VII. Geometrical control of mutual orientation of crystallites (graphotexturing)

Modern functional materials (superconductors, piezoelectrics, giant-magnetoresistance materials, *etc.*) are usually characterised by high crystallographic anisotropy of physical properties. Therefore, the desired operating characteristics of a layer can be in some

cases improved by several orders of magnitude due to biaxial texturing. A good example of the texturing effect is provided by mixed REE – barium cuprates, for which an in-plane misorientation of only 5 – 10° can cause a decrease in the density of the intergrain transport current by 10 to 100 times. Texturing of modern functional materials is related to various aspects of crystal growth in complex oxide systems. New methods of preparation of textured HTSC-coatings [176 – 178] include, in particular, the use of artificial relief of the surface of a substrate (graphotexturing, Figs 16 – 19).

At present, of particular interest is fabrication of highly textured coatings on long-length substrates or surfaces of complex shape. This problem has been inufficiently studied because of numerous technical difficulties. Most well-studied methods of deposition of textured thin films involve epitaxy.[5] High absolute values of functional parameters can also be achieved using bulk ceramic materials, which are textured using the temperature, magnetic field or electric field gradients.[4, 5] However, in these cases the specific characteristics of materials are much worse than those of the films due to imperfect texture and the presence of various macroscopic defects. A drawback of epitaxy or gradient crystallisation is that they do not allow fabrication of samples of complex shape due to a complicated procedure for preparation of substrates, which must meet severe requirements (in the case of thin films), and to brittleness of ceramics and difficulties in mechanical treatment of this material (bulk samples).

In this situation a reasonable compromise is to use thick films. To attain high specific and absolute values of the functional parameters of thick films, one should follow a hybrid approach, *i.e.*, the orientation effect of substrate (*cf.* thin films) and melt growth of large grains (*cf.* bulk materials). Unfortunately, the 'molecular' nature of epitaxy makes it efficient only for films less than 1 μm thick while conventional methods of preparation of thick films cannot be used for complete biaxial texturing.[179] In the case of thick films the orientation effect of the substrate must be based on other principles (Fig. 19). Melt crystallisation should also be modified to retain the continuity and shape of the initial layer, which undergoes melting and crystallisation, and to minimise the chemical interaction between the film and substrates.

The appearance of a film texture is a result of two main processes, *viz.*, superficial nucleation characterised by certain arrangement and orientation of seeds owing to short-range molecular fields (saturation of 'uncompensated surface bonds') and/or the motion and mutual adjustment of the 'building blocks' from the nutrient medium due to, *e.g.*, external fields and forces (see Fig. 19). As a consequence, there are two film texturing methods.

The first approach is practically implemented in the form of gas-phase or liquid-phase heteroepitaxy on single-crystalline or biaxially textured substrates. This technique is most widely used for preparation of thin films of new functional materials and heterostructures.[4, 5] However, it has significant drawbacks such as a complicated film deposition procedure, poor scaling, low performance, high cost of the deposition procedure and substrates, low deposition rate and impossibility of film deposition on two-sided items of complex shape. These drawbacks are typical of even the most recently developed methods, such as the Ion Beam Assisted Deposition (IBAD), Rolling Assisted Biaxially Textured Substrate (RABiTS) and Inclined Substrate Deposition (ISD) techniques.[180]

The second approach is independent of the substrate nature and, similarly to texturing of ceramics, does not use external factors such as thermal or magnetic field gradients and single seeds or multiseeds (see Fig. 19). Because of this, it imposes virtually no limitation on the film thickness. Usually, practical implementation of this approach requires a condensed medium, *e.g.*, a melt or a solution, to provide high thick film growth rates. The scaling problem can be solved using the principles of self-organisation or self-assembly of polycrystalline layers of multicomponent functional materials, which permit simultaneous mutual correlated

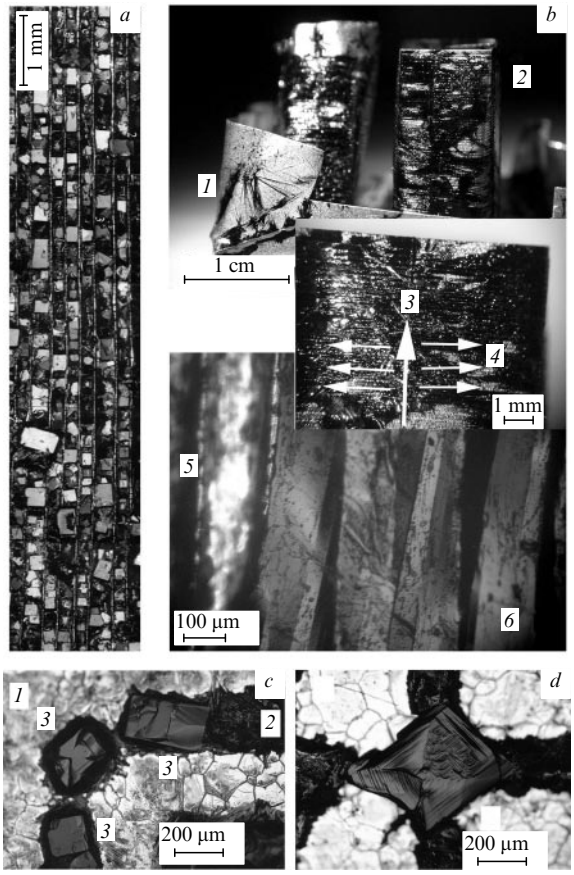


Figure 16. Micrographs of graphotextured HTSC phases.
(*a*) Biaxial texturing of polycrystalline yttrium – barium cuprate layer owing to the use of symmetrical surface relief: nearly 75% of 220 crystallites are oriented with respect to periodic striped relief (and to one another) due to nucleation near the relief elements;
(*b*) biaxially textured HTSC $Bi_2Sr_2CaCu_2O_8$ samples fabricated using silver tapes with artificial surface relief: a silver bath containing a peritectic melt of the HTSC phase (*1*), a cylinder coated with a textured HTSC layer (*2*), vertical grooves that help the melt to move upwards across the surface of the sample due to the action of capillary forces (*3*), horizontal grooves to provide (i) spillover of the melt across the surface and (ii) mutual orientation of the HTSC grains during crystallisation (*4*), a groove (*5*), ensemble of oriented crystallites (*6*);
(*c*) screen printing on silver substrate (*1*) with necessary surface structure (*2*) using an Y_2BaCuO_5 suspension followed by melt infiltration. Yttrium – barium cuprate crystallites formed on cooling (*3*) reproduce the pattern of the elements of the initial surface relief;
(*d*) surface relief (rectangular grid), which favours spontaneous formation of ⟨110⟩-oriented crystallites of mixed REE – barium cuprates (*4*).

growth on all portions of the ribbon surface. At present, these ideas are also used in nanotechnology, namely, self-assembling of monolayers causing a spontaneous formation of complex structures from the necessary building blocks; the phenomenon involves different-level energy interactions and imposition of limitations upon certain degrees of freedom of the system.[179] Research in the field of semiconductor engineering is aimed at using 'orientation filters' of the growing grains to control their growth in the desired direction.[181]

Artificial epitaxy (graphoepitaxy) was proposed nearly four decades ago for organic crystals and a number of semiconductors.[182] The method is based on the orientation effect of a microrelief created on the surface of a substrate. The relief is characterised by a certain symmetry and a period that can be several orders of magnitude greater than the lattice constant of the material. Therefore, crystals can be 'forced' to adopt a necessary

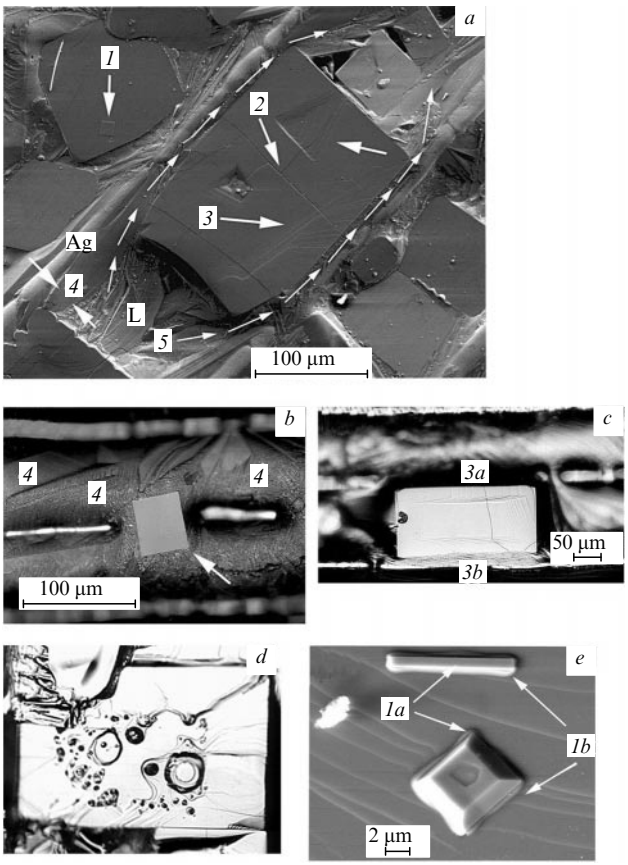


Figure 17. Micrographs of graphotextured mixed REE–barium cuprates.
Orientation of crystallites by the relief walls (*a*), a mobile crystallite solidified from melt in the early stage of growth (*b*), immobilisation of crystallite near the wall (*c*), face growth morphologies (*d*,*e*).
Notations: (*1*) barium cuprate on a crystallite face of mixed REE–barium cuprate, which interacts with growth steps (*1a*,*b*); (*2*) cracks; (*3*) (*3a*,*b*) growth steps moving from the periphery towards the centre in the case of capillary flow of the melt near the meniscus (*4*) between the relief walls and the crystallite [the direction of motion of the liquid phase, L, is shown by arrows (*5*)].

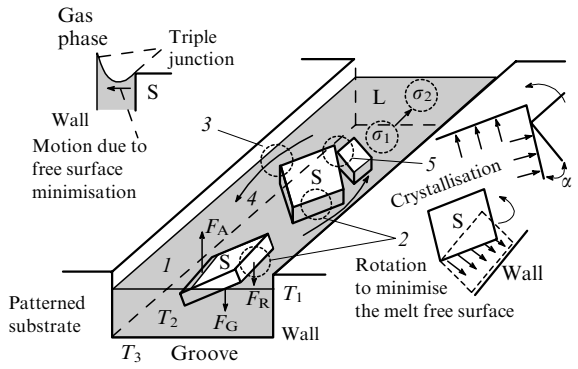


Figure 18. A model for orientation of growing crystallites.
T_1 is the temperature of the substrate surface contacting the gas phase and re-emitting heat, T_2 is the melt temperature inside the artificial relief elements (*1*), T_3 is the temperature in the bulk of the substrate, F_A is the Archimedian force, F_G is the gravity force, F_R is the surface tension force in the melt film (*2*) near crystallites (the resultant force stabilises small crystallites on the melt surface and drives them horizontally), meniscus (*3*), interacting crystallites (crystallisation pressure or a change in the meniscus shape) (*4*, *5*); σ is the surface tension depending on the component concentrations (Marangoni effect).

orientation by imposing necessary geometrical constraints on their growth. A few communications have been reported concerning the use of specific substrates, 'atomic' graphoepitaxy or application of photolithography for creation of the surface microrelief and influence of defects in the substrate on the morphology of HTSC films on polycrystalline silver.[183–185] Graphoepitaxy is efficient only for thin layers ($\sim$1 μm) and, correspondingly, only for small crystallites of size nearly 1 to 10 μm, whose orientation can be effectively controlled using methods of conventional thin-film epitaxy.

Optimisation of the deposition techniques and heat treatment regimes suitable for biaxial texturing of thick HTSC films has been the subject of recent studies.[176–178] It was established that the artificial relief must meet the following requirements: it must contain only those most efficient elements, which induce oriented growth of crystallites, and provide specified geometric constraints on the growth of crystallites in the case where the symmetry (habit) of crystallites matches the symmetry of artificial relief elements. Of great importance is also to provide conditions for nucleation near the elements of the artificial relief (otherwise, a reduced efficiency will be attained).

The artificial relief is a controllable parameter, which provides the possibility for crystallisation to occur in the desired direction. The microstructures of the samples (see Fig. 17) can be explained taking into account the effect of the artificial relief of the surface on the elementary processes occurring in the system on crystallisation, *viz*., nucleation, face growth of individual crystallites and interactions in the ensemble of the growing crystallites.

Elements of an artificial relief, which provides imposition of 'favourable' constraints on the growth of crystallites, are in fact a kind of geometrical template. A static effect of the template disturbs isotropy of the crystallising system and, finally, leads to desired orientation of crystallites in the ensemble. Unfortunately, such a template is a necessary but not sufficient condition for the formation of biaxially textured layers.

Stochastic nucleation and chaotic growth of a large number of crystallites can be among undesired factors, which preclude the growth and(or) motion of those crystallites, which could be oriented due to the effect of the artificial relief. Correspondingly, the number of crystallites per element of the artificial relief depends on both the probability density of nucleation and the characteristic size of the artificial relief elements.

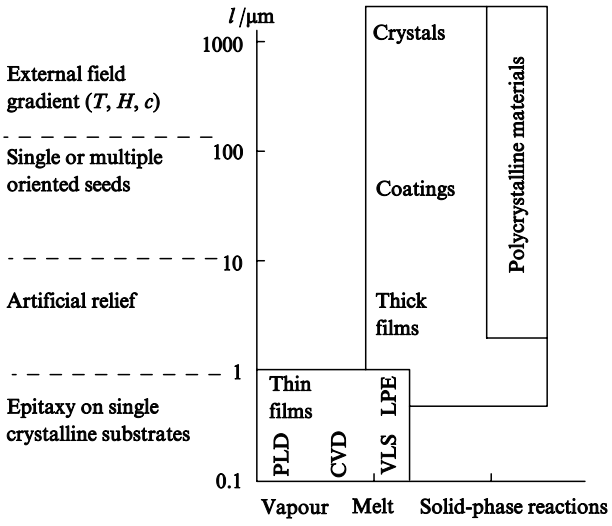


Figure 19. Main texturing techniques of polycrystalline HTSC-materials as functions of the thickness of the superconducting layer and deposition technique. Notations: PLD is Physical Layer Deposition, CVD is Chemical Vapour Deposition, VLS is Vapour Liquid Solid (mechanism) and LPE is Liquid Phase Epitaxy.

The most efficient orientation of HTSC-crystallites is attained using a simple striped relief (see Fig. 16).[176, 178] It provides (i) efficient geometric constraints on the crystal growth in the form of parallel walls of narrow grooves, (ii) a desired symmetry corresponding to the habits of the growing mixed REE–barium cuprate crystals and (iii) the density of the ensemble of crystallites, which is nearly independent of the cooling rate (because the crystallite size is limited to the groove width). At present, about 75% to 90% of the crystallites of sub-millimetre size can be readily and reproducibly aligned with a misorientation angle of less than 10° on substrates with artificial relief.

Artificial epitaxy does not use epitaxial relations for orientation of crystallites, because the technique is based on specific aspects of wetting, surface tension and meniscus, heterogeneous nucleation, redistribution of melt components, capillary effects, effects of crystallisation pressure and the topographic effect of the walls of relief elements, local temperature gradients,[176, 182] *etc*. (see Fig. 18). Clearly, high mobilities of the medium and particles in melt must provide a nearly instantaneous adjustment of orientations of the growing embryo-crystals floating on the melt surface, controlled by the relief elements, whereas the kinetics of the process depends on the adhesion, wetting of the crystallites and substrate and capillary forces and surface tension forces. The process under consideration can be practically implemented using various mechanical, electric and thermal effects that appear due to the creation of the artificial relief. The technique is convenient when using various materials and arbitrary substrates and can lead to nearly complete texturing of a polycrystalline layer in accord with the symmetry of the superficial pattern. Probably, the results reported in Refs 176–178 are among the first successful attempts to apply the method based on graphoepitaxy principles in texturing thick polycrystalline layers of complex, multicomponent systems.

VIII. Fields of practical applications of cuprates and manganites

The most promising field of practical application of the HTSC cuprates considered is design of materials for heavy-current engineering, in particular, fault current limiters (FCL). The material characteristics for an optimum FCL must be as follows:[172, 186] negligible resistance in the normal operating mode, sufficiently high resistance to limit the fault current, and high switching rate between the superconducting and resistive states. Additionally, as the fault currents are exceeded, a large amount of Joule heat releases after transition of the system to the resistive state. Therefore, the ability of the material to absorb the dissipated energy without damage should be considered as an extra necessary condition. This is possible in the case of, *e.g*., a good contact between the superconducting elements and the liquid cooling agent (this depends on the specific features of the cooling system and on the shape of the superconducting element). Respectively, high-temperature superconductors with a fabric structure having a well-developed system of regular pores (see Figs 15 *b*,*c*) to improve the contact with liquid nitrogen can be of considerable practical interest.¶

By creating a periodic and symmetrical artificial surface relief using ribbons made of commercial polycrystalline untextured silver as substrate it is possible to attain a nearly 90% mutual orientation of melt-grown HTSC crystallites in the *ab* plane.[176–178] These samples can be used as 'seed ribbons' and 'smart' seeds and for fabrication of items of complex shape. In the last-mentioned case (see Fig. 16 *b*) using a prototype device (artificially patterned HTSC coils) it was shown that the method including capillary 'suction' of melt, spillover of the melt across the surface and biaxial graphotexturing of the superconducting cuprate grains formed on cooling can be efficient in large-scale production of thick HTSC films on cheap metallic substrates in a uniform thermal field. It is possible to produce a batch of samples during one heat treatment cycle.

Growth of large superconducting crystals is mainly of academic interest to elaborate the crystal growth technique, to determine the growth mechanism and crystal parameters, *etc*. The fundamental physical characteristics can be successfully measured using small crystals. Owing to high cost and lower critical currents, the superconducting crystals can compete with neither coarse-grained ceramics used in heavy current devices nor thin films used as active elements in microelectronics.

At the same time neodymium–barium cuprate crystals with the limiting content of neodymium replacing the barium ions seem to be promising as substrate materials for fabrication of thin superconducting films. These crystals possess good dielectric properties and a small mismatch between their lattice parameters and those of the superconducting phases of other mixed REE–barium cuprates.[187] In this case, growth of large $Nd_{1.85}Ba_{1.15}Cu_3O_z$ crystals by the Czochralski method is worthwhile because the necessary surface area of polished substrates can reach a few square centimetres per device and large-scale production of this type of substrate can lead to considerable reduction of the high cost of devices for superconducting microelectronics.

This type of substrate offers some additional advantages such as chemical homogeneity (achieved using the modified Czochralski method), sufficiently high chemical stability (even in moist atmosphere), low degree of non-stoichiometry with respect to oxygen and orthorhombic unit cell. Morphology disturbance of the deposited HTSC-films at temperatures of *tetragonal–orthorhombic* transition can be prevented by oxygenation of the samples, because the anisotropy of the $R_2BaCu_3O_z$ lattice constants in the *ab* plane can act as an anisotropic strain field, which suppresses formation of twin defects in the superconducting film being deposited.

The $CaCu_xMn_{7-x}O_{12}$ solid solution can be considered as a candidate for the material to be used in magnetoresistive devices and spintronics.[188] The conductivity of $CaCu_xMn_{7-x}O_{12}$ (see Fig. 14) varies over a wide range depending on the x value and the magnetoresistance effect exhibits no pronounced thermal features. Ceramic samples synthesised from mechanically activated reactants showed the record (for this system) magnetoresistance effect of 65% at 35 K and 5 T.[20] Correspondingly, composites based on the CMR and HTSC-phases offer good prospects for practical application.[189]

Inorganic fibres provide a convenient means for fabrication of new types of materials in the form of, *e.g*., ion-conducting or catalytically active 'felts', multifilament wires or fabric (see Fig. 12 *e*). Tunnels in the structure of barium–manganese whiskers $Ba_6Mn_{24}O_{48}$ and the direction of their growth coincide. This permits practical implementation of structurally determined anisotropy of one-dimensional superionic conductivity. Usually, whiskers contain no dislocations and possess improved mechanical properties owing to the low defectiveness. In addition, studies on the behaviour of $Ba_6Mn_{24}O_{48}$ whiskers in lithium nitrate melt (see Fig. 12 *c*) showed that lithium penetrates into the structure of $Ba_6Mn_{24}O_{48}$ as a result of exchange reaction, thus inducing contraction of the unit cell along the normal to the growth direction of the whiskers. Because of this whiskers can be more stable than ceramic samples with respect to charge–discharge cycles when used as electrode materials.

Thus, the fundamental physical properties of cuprates, manganites and cupromanganites reflect the complex chemistry of copper and manganese, which predetermines structural and chemical features of these compounds. Methods of synthesis of materials with desired structures, microstructures and functional properties must be chosen allowing for this fact.

The review has been written with financial support from the Russian Foundation for Basic Research (Project Nos 04-03-32183a, 04-03-32827a and 04-03-08078ofia), the Programme 'Leading Scientific Schools' and 'Russian Universities' and from

¶ 'Super Foams' (HTSC foams) (Fig. 15) seem to have even greater prospects for being used as FCL.

the M V Lomonosov Moscow State University in the framework of Interdisciplinary Research Projects. The authors express their gratitude to N N Olejnikov, I A Presnyakov, E V Antipov, A M Abakumov, N R Khasanova, M A Novozhilov, I S Bezverkhij, V A Knot'ko and M V Makarova (Department of Chemistry, M V Lomonosov Moscow State University), E I Givargizov (Institute of Crystallography, Russian Academy of Sciences), V V Petrykin (TIT, Japan), G Schmitz and E Reddy (ACCESS e.V., Germany) and Y Shiohara (SRL ISTEC, Japan) for fruitful discussions of the results obtained.

References

1. M P Attfield *Annu. Rep. Sect. A: Inorgan. Chem.* **98** 435 (2002)
2. A Wells *Structural Inorganic Chemistry* (London: Oxford University Press, 1984)
3. D A Cardwell, D S Ginley (Eds) *Handbook of Superconducting Materials* Vols 1, 2 (Bristol, Philadelphia: IoP Publ., 2002)
4. Y Shiohara, E A Goodilin, in *Handbook on the Physics and Chemistry of Rare-Earths* Vol. 30, Ch. 189 (Eds K A Geschneidner Jr, L Eyring, M B Maple) (Amsterdam: Elsevier, 2000) p. 67
5. Yu D Tretyakov, E A Goodilin *Usp. Khim.* **69** 3 (2000) [*Russ. Chem. Rev.* **69** 1 (2000)]
6. B J Batlogg, R Buhrman, J R Clem *J. Supercond.* **10** 583 (1997)
7. J M S Skakle *Mater. Sci. Eng. R* **23** 1 (1998)
8. R J Cava, F J DiSalvo, L E Brus *Prog. Solid State Chem.* **30** 1 (2002)
9. B Raveau, A Maignan, C Martin, M Hervieu *Chem. Mater.* **10** 2641 (1998)
10. C N R Rao, A K Cheetham, R Mahesh *Chem. Mater.* **8** 2421 (1996)
11. O Yu Gorbenko, A A Bosak *Sensor* **2** 28 (2002)
12. Q Feng, H Kanoh, K Ooi *J. Mater. Chem.* **9** 319 (1999)
13. H Sato, T Enoki, J I Yamaura, N Yamamoto *Phys. Rev. B* **59** 12 836 (1999)
14. S Barbato, J L Gautier *Electochim. Acta* **46** 2767 (2001)
15. A Dyer, M Pillinger, J Newton, R Harjula, T Moller, S Amin *Chem. Mater.* **12** 3798 (2000)
16. Z Zeng, M Greenblatt, J E Sunstrom, M Croft, S Khalid *J. Solid State Chem.* **147** 185 (1999)
17. Z Zeng, M Greenblatt, M Croft *Phys. Rev. B* **58** 595 (1998)
18. I O Troyanchuk, L S Lobanovsky, N V Kasper, M Hervieu, A Maignan, C Michel, H Szymczak, A Szewczyk *Phys. Rev. B* **58** 14 903 (1998)
19. R Weht, W E Pickett *Phys. Rev. B* **65** 014415 (2001)
20. E A Pomerantseva, D M Itkis, E A Goodilin, M V Makarova, M V Lobanov, N N Oleinikov, Yu D Tretyakov *Dokl. Akad. Nauk* **388** 344 (2003) [a]
21. E V Antipov, L N Lykova, L M Kovba *Zh. Vsesoyuz. Khim. O-va im. D I Mendeleeva* **34** 458 (1989) [b]
22. N R Khasanova, A L Kharlanov, E V Antipov, L M Kovba, A A Gippius, V V Moshchalkov *Physica C* **190** 522 (1992)
23. A V Mironov, A M Abakumov, E V Antipov *Rigaku J.* **19–20** 23 (2003)
24. S N Putilin, E V Antipov, A M Abakumov, M G Rozova, K A Lokshin, D A Pavlov, A M Balagurov, D V Sheptyakov, M Marezio *Physica C* **338** 52 (2000)
25. G Van Tendeloo, O I Lebedev, R V Shpanchenko, E V Antipov *J. Electron Microsc.* **1** 23 (1997)
26. E V Antipov, S N Putilin, R V Schpanchenko, V A Alyoshin, M G Rozova, A M Abakumov, D A Mikhailova, A M Balagurov, O Lebedev, G Van Tendeloo *Physica C* **282–287** 61 (1997)
27. A M Abakumov, V L Aksenov, V A Alyoshin, E V Antipov, A M Balagurov, D A Mikhailova, S N Putilin, M G Rozova *Phys. Rev. Lett.* **80** 385 (1998)
28. A M Abakumov, M G Rozova, R V Shpanchenko, M L Kovba, S N Putilin, E V Antipov, O I Lebedev, G Van Tendeloo, E M Kopnin, J Karpinski *Physica C* **301** 155 (1998)
29. P N Oleinikov, R V Shpanchenko, M G Rozova, A M Abakumov, E V Antipov, I Khadermann, G Van Tendeloo *Zh. Neorg. Khim.* **46** 197 (2001) [c]
30. A M Alekseeva, A M Abakumov, M G Rozova, E V Antipov, J Hadermann *J. Solid State Chem.* **177** 731 (2004)
31. I F Voloshin, D A Emelianov, S O Klimonsky, V D Kuznetsov, A V Lyashenko, Yu D Tretyakov *Dokl. Akad. Nauk* **392** 779 (2003) [a]
32. S N Putulin, I Bryntse, E V Antipov *Mater. Res. Bull.* **26** 1299 (1991)
33. S N Putilin, E V Antipov, O Chmaissem, M Marezio *Nature (London)* **362** 226 (1993)
34. S N Putilin, E V Antipov, M Marezio *Physica C* **212** 266 (1993)
35. E V Antipov, S M Loureiro, C Chaillout, J J Capponi, P Bordet, J L Tholence, S N Putilin, M Marezio *Physica C* **215** 1 (1993)
36. M Nunez-Regueiro, J L Tholence, E V Antipov, J J Capponi, M Marezio *Science* **262** 97 (1993)
37. J J Capponi, J L Tholence, C Chaillout, M Marezio, P Bordet, J Chenavas, S M Loureiro, E V Antipov, E M Kopnin, M F Gorius, M Nunez-Regueiro, B Souletie, P Radaelli, F Gerhards *Physica C* **235–240** 146 (1994)
38. V A Alyoshin, D A Mikhailova, E V Antipov *Physica C* **271** 197 (1996)
39. A M Balagurov, D V Sheptyakov, V L Aksenov, E V Antipov, S N Putilin, P G Radaelli, M Marezio *Phys. Rev. B* **59** 7209 (1999)
40. O Chmaissem, Q Huang, E V Antipov, S N Putilin, M Marezio, S M Loureiro, J J Capponi, J L Tholence, A Santoro *Physica C* **217** 265 (1993)
41. G Van Tendeloo, C Chaillout, J J Capponi, M Marezio, E V Antipov *Physica C* **223** 219 (1994)
42. V L Aksenov, A M Balagurov, B N Savenko, V P Glazkov, I N Goncharenko, V A Somenkov, E V Antipov, S N Putilin, J J Capponi *High Pres. Res.* **14** 127 (1995)
43. G Fuchs, K A Nenkov, A Attenberger, K Luders, M Baenitz, C Ecker, K Kajikawa, E V Antipov, H R Khan *Physica C* **355** 299 (2001)
44. P Schilbe, K Lmders, M Baenitz, D A Pavlov, I Bryntse, A Abakumov, E V Antipov *Physica C* **391** 298 (2003)
45. P Schilbe, K Lmders, M Baenitz, D A Pavlov, A Abakumov, E V Antipov *Physica C* **388–389** 247 (2003)
46. J Karpinski, S M Kazakov, M Augst, A Mironov, M Mali, J Roos *Phys. Rev. B* **64** 094 518 (2001)
47. P Bordet, F Duc, S Le Floch, J J Capponi, E Alexandre, M Rosa-Nunes, S Putilin, E V Antipov *Physica C* **271** 189 (1996)
48. D V Fomichev, O G D'yachenko, A V Mironov, E V Antipov *Physica C* **245** 25 (1994)
49. S F Pashin, E V Antipov, L M Kovba, Yu Ya Skolis *Sverkhprovodimost: Fiz. Khim. Tekh.* **2** 102 (1989)
50. D A Mikhailova, V A Alyoshin, E V Antipov, J Karpinski *J. Solid State Chem.* **146** 151 (1999)
51. V A Alyoshin, D A Mikhailova, E V Antipov, A S Monayenkova, A A Popova, L A Tiphlova, J Karpinski *J. Alloys Compd.* **284** 108 (1999)
52. V A Alyoshin, D A Michailova, E B Rudnyi, E V Antipov *Physica C* **383** 59 (2002)
53. S N Mudretsova, A F Maiorova, A A Bosak, O Yu Gorbenko, A R Kaul, N A Babushkina, L M Belova *Zh. Fiz. Khim.* **74** 1765 (2000) [d]
54. P E Kazin, D D Zaitsev, Yu D Tretyakov *Dokl. Akad. Nauk* **385** 355 (2002) [a]
55. P E Kazin, A S Karpov, Yu D Tretyakov, M Jansen *Solid State Sci.* **3** 285 (2001)
56. P E Kazin, Yu D Tretyakov, V V Lennikov, M Jansen *J. Mater. Chem.* **11** 168 (2001)
57. P E Kazin, A A Kovalevskii, V V Poltavets, Yu D Tretyakov, M Yanzen *Neorg. Mater.* **37** 1383 (2001) [e]
58. M V Lobanov, A M Balagurov, V Ju Pomjakushin, P Fisher, M Gutmann, A M Abakumov, O G D'yachenko, E V Antipov, O I Lebedev, G Van Tendeloo *Phys. Rev. B* **61** 8941 (2000)
59. O A Shlyakhtin, Y-J Oh, Yu D Tretyakov *Solid State Commun.* **117** 261 (2001)
60. O A Shlyakhtin, Y-J Oh, Yu D Tretyakov *J. Eur. Ceram. Soc.* **20** 2047 (2000)

61. A M Abakumov, A V Mironov, V A Govorov, M V Lobanov, M G Rozova, E V Antipov, O I Lebedev, G Van Tendeloo *Solid State Sci.* **5** 1117 (2003)
62. O Yu Gorbenko, A R Kaul, I V Pogosova, S N Polyakov, E V Kolosova, S A Pozigun, V I Scritny *Mater. Sci. Eng. B* **17** 157 (1993)
63. W Decker, Yu Erokhin, O Gorbenko, I Graboy, A Kaul, A Nurnberg, M Pulver, R Stolle, G Wahl *J. Alloys Compd.* **195** 291 (1993).
64. O Yu Gorbenko, W Decker, G Wahl *J. Phys. IV* **3** 25 (1993)
65. W Decker, A Nurnberg, M Pulver, R Stolle, G Wahl, Yu Erokhin, O Gorbenko, I Graboy, A Kaul *Physica C* **209** 195 (1993)
66. O Yu Gorbenko, V N Fuflyigin, Yu Yu Erokhin, I E Graboy, A R Kaul, Yu D Tretyakov, L Klippe, G Wahl *J. Mater. Chem.* **4** 1585 (1994)
67. S V Samoilenkov, O Yu Gorbenko, A R Kaul, Yu D Tretyakov *Sverkhprovodimost* **8** 113 (1995)
68. S V Samoylenkov, O Yu Gorbenko, A R Kaul *Physica C* **267** 74 (1996)
69. S V Samoylenkov, O Yu Gorbenko, A R Kaul, Y A Rebane, V L Svetchnikov, H W Zandbergen *J. Alloys Compd.* **251** 342 (1997)
70. S O Klimonsky, S V Samoilenkov, O Yu Gorbenko, D A Emelianov, A V Lyashenko, S R Lee, A R Kaul, Yu D Tretyakov, D G Andrianov, A V Kalinov, I F Voloshin *Physica C* **383** 37 (2002)
71. G A Tsirlina, S N Putilin, O A Petrii, E V Antipov, Ya G Ponomarev, Kh T Rakhimov *Sverkhprovodimost: Fiz. Khim. Tekh.* **4** 1580 (1991)
72. O I Lebedev, G Van Tendeloo, A M Abakumov, S Amelinckx, B Leibold, H-U Habermeier *Philos. Mag. A* **79** 1461 (1999)
73. O Yu Gorbenko, A R Kaul, N A Babushkina, L M Belova *J. Mater. Chem.* **7** 747 (1997)
74. O Yu Gorbenko, R V Demin, L I Koroleva, A R Kaul, R Shimchak *Fiz. Tv. Tela* **40** 290 (1998) [f]
75. N A Babushkina, L M Belova, D I Khomskii, K I Kugel, O Yu Gorbenko, A R Kaul *Phys. Rev. B* **59** 6994 (1999)
76. O Yu Gorbenko, A A Bosak, V A Amelichev, A Yu Ganin, I E Graboy, A R Kaul, G Wahl, H W Zandbergen *J. Phys. IV* **9** 659 (1999)
77. O Yu Gorbenko, A R Kaul, A A Bosak, I E Graboy, H W Zandbergen, V L Svetchnikov, N A Babushkina, L M Belova, K I Kugel *Solid State Commun.* **114** 407 (2000)
78. A A Bosak, O Yu Gorbenko, A R Kaul, I E Graboy, C Dubourdieu, J P Senateur, H W Zandbergen *J. Magn. Magn. Mater.* **211** 61 (2000)
79. M Bibes, O Gorbenko, B Martinez, A Kaul, J Fontcuberta *J. Magn. Magn. Mater.* **211** 47 (2000)
80. O Yu Gorbenko, I E Graboy, A R Kaul, H W Zandbergen *J. Magn. Magn. Mater.* **211** 97 (2000)
81. V A Amelitchev, B Güttler, O Yu Gorbenko, A R Kaul, A A Bosak, A Yu Ganin *Phys. Rev. B* **63** 104430 (2001)
82. B Guettler, V A Amelitchev, O Yu Gorbenko *Phase Transitions* **76** 63 (2003)
83. N A Babushkina, L M Belova, O Yu Gorbenko, A R Kaul, A A Bosak, V I Ozhogin, K I Kugel *Nature (London)* **391** 159 (1998)
84. L M Belova, N A Babushkina, O Yu Gorbenko, A R Kaul, K I Kugel, D I Khomskii *Physica B* **284–288** 1434 (2000)
85. N N Loshkareva, Yu P Sukhorukov, E A Gan'shina, E V Mostovshchikova, R Yu Kumaritova, A S Moskvin, Yu D Panov, O Yu Gorbenko, A R Kaul *Zh. Eksp. Teor. Fiz.* **119** 533 (2001) [g]
86. A M Balagurov, V Yu Pomjakushin, D V Sheptyakov, V L Aksenov, N A Babushkina, L M Belova, O Yu Gorbenko, A R Kaul *Eur. Phys. J. B* **19** 215 (2001)
87. M Baran, S L Gnatchenko, O Yu Gorbenko, A R Kaul, R Szymczak, H Szymczak *Phys. Rev. B* **60** 9244 (1999)
88. Yu P Sukhorukov, N N Loshkareva, E A Gan'shina, A R Kaul, O Yu Gorbenko, K A Fatieva *Pis'ma Zh. Tech. Fiz.* **25** 6 (1999) [h]
89. E A Gan'shina, O Yu Gorbenko, A G Smechova, A R Kaul, N A Babushkina, L M Belova *J. Phys.: Condens. Matter* **12** 2857 (2000)
90. T Mertelj, A A Bosak, O Yu Gorbenko, A R Kaul, D Mihailovic *Int. J. Mod. Phys. B* **14** 3584 (2000)
91. A A Bosak, A A Kamenev, I E Graboy, S V Antonov, O Yu Gorbenko, A R Kaul, C Dubourdieu, J P Senateur, V L Svechnikov, H W Zandbergen, B Hollinder *Thin Solid Films* **400** 149 (2001)
92. A A Gippius, E V Antipov, O Klein, K Lüders *Physica B* **284–288** 935 (2000)
93. A A Gippius, E N Morozova, E V Antipov, A M Abakumov, M G Rozova, K Lmders, W Hoffmann, G Buntkowsky, O Klein *Phys. Rev. B* **61** 14370 (2000)
94. A A Gippius, E V Antipov, W Hoffmann, K Lüders, G Buntkowsky *Phys. Rev. B* **59** 654 (1999)
95. W Hoffmann, H Breitzke, M Baenitz, M Heinze, K Lmders, G Buntkowsky, H H Limbach, E V Antipov, A A Gippius, O Loebich, H R Khan, M Paranthaman, J R Thompson *Physica C* **227** 225 (1994)
96. Yu D Tretyakov *Usp. Khim.* **72** 731 (2003) [*Russ. Chem. Rev.* **72** 651 (2003)]
97. Yu D Tretyakov *Khim. Ros.* **9** 11 (2000)
98. P E Kazin, Yu D Tretyakov *Usp. Khim.* **72** 960 (2003) [*Russ. Chem. Rev.* **72** 849 (2003)]
99. O Yu Gorbenko, V N Fuflygin, A R Kaul *Sverkhprovodimost: Issled. Razrab.* **5–6** 38 (1995)
100. O Yu Gorbenko, S V Samoilenkov *Sverkhprovodimost* **8** 800 (1995)
101. A M Abakumov, M G Rozova, E I Ardashnikova, E V Antipov *Usp. Khim.* **71** 442 (2002) [*Russ. Chem. Rev.* **71** 383 (2002)]
102. E V Antipov, V A Aleshin *Zh. Neorg. Khim.* **47** 530 (2002) [c]
103. A M Abakumov, M G Rozova, S N Putilin, E V Antipov *Naukoemkie Tekhnol.* **1** 50 (2003)
104. S M Loureiro, J J Capponi, E V Antipov, M Marezio, in *Studies of High Temperature Superconductors* Vol. 25 (New York: Nova Science Publisher, 1997) p. 229
105. E V Antipov, A M Abakumov, S N Putilin *Supercond. Sci. Technol.* **15** R31 (2002)
106. A M Abakumov, E V Antipov, L M Kovba, E M Kopnin, S N Putilin, R V Shpanchenko *Usp. Khim.* **64** 769 (1995) [*Russ. Chem. Rev.* **64** 719 (1995)]
107. E V Antipov, Doctoral Thesis in Chemical Sciences, Moscow State University, Moscow, 1997
108. A A Kiselev (Ed.) *Vysokotemperaturnaya Svekhprovodimost'. Fundamental'nye i Prikladnye Issledovaniya* (High-Temperature Superconductivity. Fundamental and Applied Investigations) (Leningrad: Mashinostroenie, 1990) No. 1
109. H B Brom, J Zaanen, in *Handbook of Magnetic Materials* (Ed. K H J Buschow) (Amsterdam: Elsevier, 2003) p. 379
110. A Läuchli, G Schmid, M Troyer *Phys. Rev. B* **67** 100409(R) (2003)
111. T M Rice *Z. Phys. B* **103** 165 (1997)
112. O Tamada, H Paulus, H Fuess, N Yamamoto, S Muranaka *J. Solid State Chem.* **108** 112 (1994)
113. V G Zubkov, A P Tyutyunnik, I F Berger, V I Voronin, G V Bazuev, C A Moore, P D Battle *J. Solid State Chem.* **167** 453 (2002)
114. M A Subramanian, A P Ramirez, G H Kwei *Solid State Ionics* **108** 185 (1998)
115. M M Cruz, M D Carvalho, A Casaca, G Bonfait, F M Costa, M Godinho *J. Magn. Magn. Mater.* **226–230** 800 (2001)
116. V V Petrykin, E A Goodilin, J Hester, E A Trofimenko, N N Oleynikov, M Kakihana, Yu D Tretyakov *Physica C* **340** 16 (2000)
117. V V Petrykin, E A Goodilin, J Hester, E A Trofimenko, M Kakihana, N N Oleynikov, Y D Tretyakov *Physica C* **357** 388 (2001)
118. E A Goodilin, I A Presnyakov, M V Tarasov, S N Mudretsova, A F Maiorova, J Hester, N N Oleinikov, Yu D Tretyakov *Dokl. Akad. Nauk* **373** 160 (2000) [a]
119. K V Didenko, D V Peryshkov, E A Goodilin, I A Presnyakov, E A Pomerantseva, Yu D Tretyakov *Dokl. Akad. Nauk* **387** 343 (2002) [a]
120. D V Peryshkov, E A Goodilin, M V Makarova, E A Pomerantseva, S N Mudretsova, A F Maiorova, Yu D Tretyakov *Dokl. Akad. Nauk* **387** 491 (2002) [a]

121. D V Peryshkov, E A Goodilin, M V Makarova, S N Mudretsova, A F Maiorova, Yu D Tretyakov *Dokl. Akad. Nauk* **383** 651 (2002) [a]
122. E A Pomerantseva, D M Itkis, I A Presnyakov, E A Goodilin, J Hester, N N Oleinikov, Yu D Tretyakov *Dokl. Akad. Nauk* **387** 207 (2002) [a]
123. M F Limonov, E A Goodilin, X Yao, S Tajima, Y Shiohara, Yu E Kitaev *Phys. Rev. B* **58** 12368 (1998)
124. Yu D Tretyakov, E A Goodilin *Curr. Appl. Phys.* **3** 377 (2003)
125. Yu D Tretyakov, E A Goodilin *Physica B* **321** 249 (2002)
126. Z Hommonay, in *Mössbauer Spectroscopy of Sophisticated Oxides* (Eds A Vertes, Z Hommonay) (Budapest: Akademiai Kiado, 1997) p. 159
127. A V Kravchenko, E A Goodilin, I S Bezverkhii, D M Predtechenskaya, N N Oleinikov, Yu D Tretyakov *Zh. Neorg. Khim.* **45** 983 (2000) [c]
128. Ph Boullay, M Hervieu, B Raveau *J. Solid State Chem.* **132** 239 (1997)
129. H H Hamdeh, J C Ho, S A Oliver, J G Lin, S Y Lin, P C Kuo, C Y Huang *J. Magn. Magn. Mater.* **232** 175 (2001)
130. F Studer, N Nguyen, O Toulemonde, A Ducouret *Int. J. Inorg. Mater.* **2** 671 (2000)
131. I D Fawcett, M V Gabriel, M Greenblatt, M Croft, I Nowik *Solid State Sci.* **2** 821 (2000)
132. A Nath, V Chechersky, R L Greene *J. Solid State Chem.* **155** 116 (2000)
133. V Chechersky, A Nath, I Isaac, J P Franck, K Ghosh, R L Greene *Phys. Rev. B* **63** 52411 (2001)
134. H S Horowitz, J M Longo *Mater. Res. Bull.* **13** 1359 (1978)
135. E A Goodilin, E A Pomerantseva, O Yu Gorbenko, V V Petrykin, V V Poltavets, A V Knot'ko, A M Abakumov, N N Oleinikov, Yu D Tretyakov, M Kakikhana *Dokl. Akad. Nauk* **372** 100 (2000) [a]
136. Yu D Tretyakov, E A Goodilin *Zh. Neorg. Khim.* **46** 203 (2001) [c]
137. E Goodilin, A Oka, J G Wen, Y Shiohara, M Kambara, T Umeda *Physica C* **299** 279 (1998)
138. E Goodilin, M Kambara, T Umeda, Y Shiohara *Physica C* **289** 37 (1997)
139. M Kambara, M Tagami, X Yao, E Goodilin, Y Shiohara, T Umeda *J. Am. Ceram. Soc.* **81** 2116 (1998)
140. E Goodilin, M Kambara, T Umeda, Y Shiohara *Physica C* **289** 251 (1997)
141. E A Goodilin, N N Oleynikov, G Yu Popov, V A Shpanchenko, E V Antipov, G V Balakirev, Yu D Tretyakov *Physica C* **272** 65 (1996)
142. Y Yamada, M Nakamura, Y Shiohara, S Tanaka *J. Cryst. Growth* **148** 241 (1995)
143. M Kambara, X Yao, M Nakamura, Y Shiohara, T Umeda *J. Mater. Res.* **12** 2866 (1997)
144. X Yao, Y Shiohara *Supercond. Sci. Technol.* **10** 249 (1997)
145. M Egami, Y Shiohara, in *Advances in Superconductivity* Vol. 9 (Eds S Nakajima, M Murakami) (Tokyo: Springer, 1997) p. 809
146. X Yao, E A Goodilin, T Izumi, Y Shiohara *J. Mater. Res.* **16** 529 (2001)
147. X Yao, E Goodilin, Y Yamada, H Sato, Y Shiohara *Appl. Superconduct.* **6** 175 (1998)
148. Z Zou, J Ye, K Oka, Y Nishihara *Phys. Rev. Lett.* **80** 1074 (1998)
149. H Zhang, G Wang, H Wu *J. Cryst. Growth* **154** 293 (1995)
150. E A Goodilin, A P Soloshenko, V V Lennikov, A V Knot'ko, N N Oleynikov, Y D Tretyakov, in *Proceedings of the First Regional Conference on Magnetic and Superconducting Materials, MSM'99* (Eds M Akhavan, J Jensen, K Kitazawa) (Singapore: World Scientific, 2000) p. 167
151. E A Goodilin, A P Soloshenko, V V Lennikov, A V Knot'ko, D A Vetoshkin, N N Oleinikov, Yu D Tretyakov *Zh. Neorg. Khim.* **45** 917 (2000) [c]
152. S Lee, K-J Kwon, W-S Kim, S-I Lee *Physica C* **251** 149 (1995)
153. C Kloc, S W Cheong, P Matl *J. Cryst. Growth* **191** 294 (1998)
154. R Suryanarayanan, G Dhalenne, A Revcolevschi, W Prellier, J-P Renard, C Dupas, W Caliebe, T Chatterji *Solid State Commun.* **113** 267 (2000)
155. V A Cherepanov, L Yu Barkhatova, V I Voronin *J. Solid State Chem.* **134** 38 (1997)
156. W H McCarroll, K V Ramanuajachary, I D Fawcett, M Greenblatt *J. Solid State Chem.* **145** 88 (1999)
157. D Zhu, H Zhu, Y Zhang *J. Crystal Growth.* **249** 172 (2002)
158. X Wang, Y Li *Chem. Eur. J.* **9** 300 (2003)
159. C Xu, X Zhao, G Wang *J. Nanosci. Nanotech.* **3** 406 (2003)
160. E A Goodilin, N N Oleinikov, S R Li, Yu D Tretyakov *Zh. Neorg. Khim.* **39** 1043 (1994) [c]
161. C Zener *Phys. Rev.* **82** 403 (1951)
162. R V Krishnan, A Banerjee *J. Phys.: Condens. Matter* **12** 3835 (2000)
163. A J Millis *Nature (London)* **392** 147 (1998)
164. E L Nagaev *Usp. Fiz. Nauk* **168** 918 (1998) [*Physics-Uspekhi* **41** 831 (1998)]
165. M V Krasil'nikova *Zh. Tekhn. Fiz.* **72** 30 (2002) [i]
166. E A Goodilin, D V Pyorishkov, A V Knot'ko, V V Lennikov, N N Oleynikov, Y D Tretyakov *Physica C* **349** 278 (2001)
167. E A Goodilin, G Yu Popov, N N Oleinikov, G P Murav'eva, P E Kazin, Yu D Tretyakov *Dokl. Akad. Nauk* **344** 773 (1995) [a]
168. E S Reddy, G J Schmitz *Supercond. Sci. Technol.* **15** L21 (2002)
169. E S Reddy, J G Noudem, E A Goodilin, M Tarka, G J Schmitz *Supercond. Sci. Technol.* **16** 402 (2003)
170. J G Noudem, E S Reddy, E A Goodilin, M Tarka, M Noe, G J Schmitz *Physica C* **372–376** 1631 (2002)
171. E S Reddy, E A Goodilin, M Tarka, M Zeisberger, G J Schmitz *Physica C* **372–376** 1200 (2002)
172. J G Noudem, E S Reddy, M Tarka, M Noe, E A Goodillin, G J Schmitz *Physica C* **366** 93 (2002)
173. G J Schmitz, E S Reddy, E A Goodilin *Physica C* **378–381** 607 (2002)
174. J G Noudem, E S Reddy, E A Goodilin, M Tarka, M Noe, G J Schmitz *Physica C* **372–376** 1187 (2002)
175. G J Schmitz, O Kugeler *Physica C* **275** 205 (1997)
176. E A Goodilin, E S Reddy, J G Noudem, M Tarka, G J Schmitz *J. Cryst. Growth.* **241** 512 (2002)
177. E A Goodilin, E S Reddy, J G Noudem, M Tarka, G J Schmitz *Physica C* **372–376** 842 (2002)
178. Yu D Tretyakov, E A Goodilin, E S Reddi, G J Schmitz *Kristallografiya* **49** 283 (2004) [j]
179. F Schreiber *Prog. Surface Sci.* **65** 151 (2000)
180. S Tanaka *Physica C* **392–396** 1 (2003)
181. H Tanabe, C M Chen, H A Atwater *Appl. Phys. Lett.* **77** 4325 (2000)
182. E I Givargizov, in *Handbook of Crystal Growth* Pt. 3b (Ed. D T J Hurle) (Amsterdam: Elsevier, 1994) p. 941
183. H U Habermeier *J. Supercond.* **13** 871 (2000)
184. S Miyazawa, M Mukaida *Appl. Phys. Lett.* **64** 2160 (1994)
185. W D Dozier, C E Platt *App. Phys. Lett.* **62** 2048 (1993)
186. M Chen, L Donzel, M Lakner, W Paul *J. Eur. Ceram. Soc.* **24** 1815 (2004)
187. F M Saba, M Tagami, E A Goodilin, Y Shiohara, Y Enomoto *IEEE Trans. Appl. Supercond.* **10** 1662 (2000)
188. S A Wolf, D D Awschalom, R A Buhrman, J M Daughton, S von Molna, M L Roukes, A Y Chtchelkanova, D M Treger *Science* **294** 1488 (2001)
189. O Yu Gorbenko, I E Graboy, A A Bosak, V A Amelichev, A Yu Ganin, A R Kaul, G Wahl, H W Zandbergen *J. Phys. IV* **9** 659 (1999)

[a] — *Dokl. Chem. (Engl. Transl.)*
[b] — *Mendeleev Chem. J. (Engl. Transl.)*
[c] — *Russ. J. Inorg. Chem. (Engl. Transl.)*
[d] — *Russ. J. Phys. Chem. (Engl. Transl.)*
[e] — *Inorg. Mater. (Engl. Transl.)*
[f] — *Phys. Solid State (Engl. Transl.)*
[g] — *J. Exp. Theor. Phys. (Engl. Transl.)*
[h] — *J. Tech. Phys. Lett. (Engl. Transl.)*
[i] — *J. Tech. Phys. (Engl. Transl.)*
[j] — *Crystallogr. Rep. (Engl. Transl.)*